Journal of Imaging Science and Technology® 65(4): 040405-1–040405-23, 2021.

On-demand Electrohydrodynamic Jetting of an Ethylene Glycol and Water Mixture—System of Controlled Picoliter Fluid Deposition

J. F. Dijksman▲
University of Twente, Faculty Science and Technology, Physics of Fluids, Drienerlolaan 5, 7522NB Enschede, The Netherlands
E-mail: j.f.dijksman@kpnmail.nl

U. Stachewicz
AGH University of Science and Technology, Faculty of Metals Engineering and Industrial Computer Science, Al. A. Mickiewicza 30, 30-059 Kraków, Poland

Abstract. *On-demand electrohydrodynamic jetting also called electrohydrodynamic atomization (EHDA) is a method to jet small amounts of fluid out of a nozzle with a relatively large diameter by switching on and off an electrical field between the nozzle and the substrate. The total amount of volume deposited is up to 5 pL. The set-up consists of a vertically placed glass pipette with a small nozzle directed downward and a flat substrate placed close to the end of the nozzle. Inside the pipette, an electrode is mounted close to the entrance of the nozzle. The electrode is connected to a high voltage power amplifier. Upon switching on the electrical field, the apparent surface tension drops, the meniscus deforms into a cone and fluid starts to flow toward the nozzle deforming the meniscus. At a certain moment the cone reaches the Taylor cone dimensions and from its tip a jet emerges that decomposes into a stream of charged fL droplets that fly toward the substrate. This process stops when the pulse is switched off. After switching off, the meniscus returns slowly to its equilibrium position. The process is controlled by different time constants, such as the slew rate of the power amplifier and the RC time of the electrical circuit composed of the electrical resistance in the fluid contained in the nozzle between the electrode and the meniscus, and the capacitance of the gap between the meniscus and the flat substrate. Another time constant deals with the fluid flow during the growth of the meniscus, directly after switching on the pulse. This fluid flow is driven by hydrostatic pressure and opposed by a viscous drag in the nozzle. The final fluid flow during droplet formation is governed by the balance between the drag of the charge carriers inside the fluid, caused by the current associated with the charged droplets leaving the meniscus and the viscous drag. These different phenomena will be discussed theoretically and compared to experimental results.* © *2021 Society for Imaging Science and Technology.*
[DOI: 10.2352/J.ImagingSci.Technol.2021.65.4.040405]

1. INTRODUCTION

1.1 *Statement of Problem*

There are two principally different ways to generate an electrospray—a spray of small electrically charged droplets generated by applying an electrical potential between a pending fluid meniscus of an electrically conducting fluid and a grounded plate. The size of the pending meniscus is much larger than the droplets generated. Electrical conduction in liquids is due to mobile ions [1]. The first way of working is to generate a constant flow rate by means of a pump through a nozzle made of metal [2–4] and subject the meniscus to a constant or periodically changing electrical field. This method is used, e.g., for coating purposes, where large amounts of charged droplets are deposited onto a substrate. Because of the large distance between the nozzle and the substrate, the charged droplets form a spray rather than a jet because of Coulomb repulsion. The second one is to generate droplets on demand from a pending meniscus attached to the inner rim of a small nozzle at the end of an electrically insulating glass capillary. The substrate is placed at a short distance from the nozzle, in this way we avoid the electrospray formation and stay in the jetting mode. Inside the capillary, an electrode is mounted close to the entrance region of the nozzle. During idling, the fluid contained in the capillary is kept in place by surface tension. In this case, no syringe pump or any other fluid flow control system is used to generate the flow rate. It is simply a pressure driven system of fluid flow. Upon pulsing, between the electrode inside the capillary and the plate kept at ground potential, a square voltage pulse is applied [5–13]. In this way, it is possible to generate on demand an electrified jet that decomposes into a stream of small fL droplets by Rayleigh–Plateau–Weber instability [14, 15]. As the nozzle is placed close to the substrate, the jet and the droplets follow an almost straight trajectory as Coulomb repulsion has no time to become active. The total volume deposited is composed of a number of these small droplets and can be as large as several picoliters. Small in this context means small with respect to the nozzle radius. On its turn the radius of the nozzle is small with respect to the capillary length [16], so gravity effects on the shape of the meniscus can be ruled out. The time between pulses can be variable making it possible to print patterns or images on a moving grounded substrate. Electrospraying is one of the possibilities to make small droplets; see the extensive review report of Montanero and Cañán-Calvo [17].

▲ IS&T Member.

Received May 10, 2021; accepted for publication Aug. 3, 2021; published online Aug. 25, 2021. Associate Editor: Jihoon Kim.
1062-3701/2021/65(4)/040405/23/$25.00

As there is no flow control device present, the flow generated depends solely on the change in effective surface tension due to charging of the pending meniscus, the hydrostatic pressure, the surface tension high up in the capillary and electrostatic and electrokinetic forces. In metal capillaries, the electrokinetic force is absent, because the current is directly guided to the meniscus through the low resistance metal nozzle. Glass is electrically insulating; therefore, in a liquid-filled glass capillary the current has to flow from the tip of an electrode mounted inside the capillary through the liquid toward the meniscus, dragging along ions. Dragging means force, which in this case is the electrokinetic force [18].

Generating on-demand electrohydrodynamic jetting by electrical pulsing is sometimes referred to as Single Event Electrospraying or a Single Electrospraying Event (SEE) [5–11]. Applications are the deposition of extremely small amounts of solvents for the manufacturing of biosensors, controlled electrospraying of substances dissolved in water, e.g., for the treatment of patients suffering from COPD, etc. [19]. Electrohydrodynamic jetting is an important process in Electrospinning, especially for manufacturing hollow fibers [20], printing of ultrafine tracks of conducting material on printed circuit boards and glass substrates [21–23]. It is often called direct electrospinning [23] or writing [24] where various more viscous fluids are used in the form of polymer solutions, which is often affected by the experimental settings [25–27]. This method has a wide range of applications to produce scaffolds for tissue engineering [28], skin patches [29], drug delivery systems [30, 31], in energy [32], water harvesting [33] and smart textiles [34].

On-demand electrohydrodynamic jetting is characterized by:

- Driven by a single pulse.
- Distance between nozzle front and substrate is small.
- Fluid flow controlled by the equilibrium of hydrostatics, capillary effects, viscous drag, capacitance and electrokinetic forcing. No volume rate of flow controller is needed.
- Within the time interval of the pulse (the pulse time) it takes considerable time after switching on the potential before the jetting actually starts. In the meantime, fluid flows downward deforming the meniscus strongly.
- The electrohydrodynamic jetting starts with a thin jet emerging from the tip of a cone. The jet decomposes into small droplets. As the distance between the nozzle and the substrate is small, the effect of Coulomb repulsion is negligible and the trajectory of jet and droplets is almost straight.
- The droplets have much smaller dimensions compared to the size of the meniscus or the diameter of the nozzle. The volume deposited is the result of many small droplets.
- By adjusting the pulse time, the amount of fluid deposited can be controlled.
- Pulses can be applied after each other. Up to a certain frequency, on-demand electrohydrodynamic jetting (or SEE) is not dependent on the repeat rate of the electrical pulses. This holds true up to a few hundreds of Hz.

In this article, we will develop a theoretical model that explains in detail all aspects of on-demand electrohydrodynamic jetting, also known as Single Event Electrospraying. It is about understanding the hydrostatics and electrostatics of the equilibrium state during the time interval in between pulses and the hydrodynamic effects powered by electrodynamical and electrokinetic phenomena during applying the electrical pulse. Next to the hydrostatic pressure head, electrokinetic forcing is a key effect that powers this on-demand deposition method. As current is directly coupled to the time rate of change of capacitance, detailed analyses are given of the capacitances of a spherical fluid dome surface and a conical surface. Electrokinetic effects are controlling the start-up ("kick-start") and the strong deceleration of the fluid column directly after switching off ("emergency stop"). Reference will be made to experimental results obtained by us previously [5–11].

The analyses are confined to Newtonian liquids. This theory also applies to poorly electrically conducting fluids. Jet break-up and the stability of a stream of charged droplets is outside the scope of this article; see [35] for a detailed analysis.

2. MATERIALS AND METHODS

2.1 *Experimental Set-up*

In order to compare our theoretical findings, we will refer to a number of experiments carried out by Stachewicz [11]. The experiments were done with Microdrop Autodrop AD-H-501 glass micropipettes (Germany), mounted with the nozzle pointing downward. At a small distance a plate is fixed, kept at ground potential. A schematic of the set-up is shown in Figure 1 together with additional data. The electrical scheme is depicted in Figure 2. The nozzle has a diameter of 50 μm ($R_{nozzle} = 25$ μm), the inner diameter of the glass capillary is 0.8 mm ($R_{cap} = 0.4$ mm). Inside the micropipette the change from capillary to nozzle is gradual. Although not perfectly straight, the length of narrowest part, referred to as nozzle length, measures $L_{nozzle} = 1.2$ mm. The micropipette is connected to an under-pressure controller via a Teflon tube. Under-pressure control is sometimes needed to fix the meniscus position or to prevent the nozzle from leaking. The length of the fluid column inside the capillary measures 21.3 cm. The fluid column extends into the Teflon tube.

Inside the fluid column, an electrode is mounted of which the tip is close to the nozzle entrance, the distance between the tip and the nozzle front equals $D_{tip} = 1.6$ mm. By means of a power amplifier (Trek Inc Model 5/80, Acal Bfl, Sweden), an electrical square pulse can be applied to the system. The pulse is given by its height in volts and duration in μs. A critical parameter is the slew rate, the rate at which the set pulse height is reached.

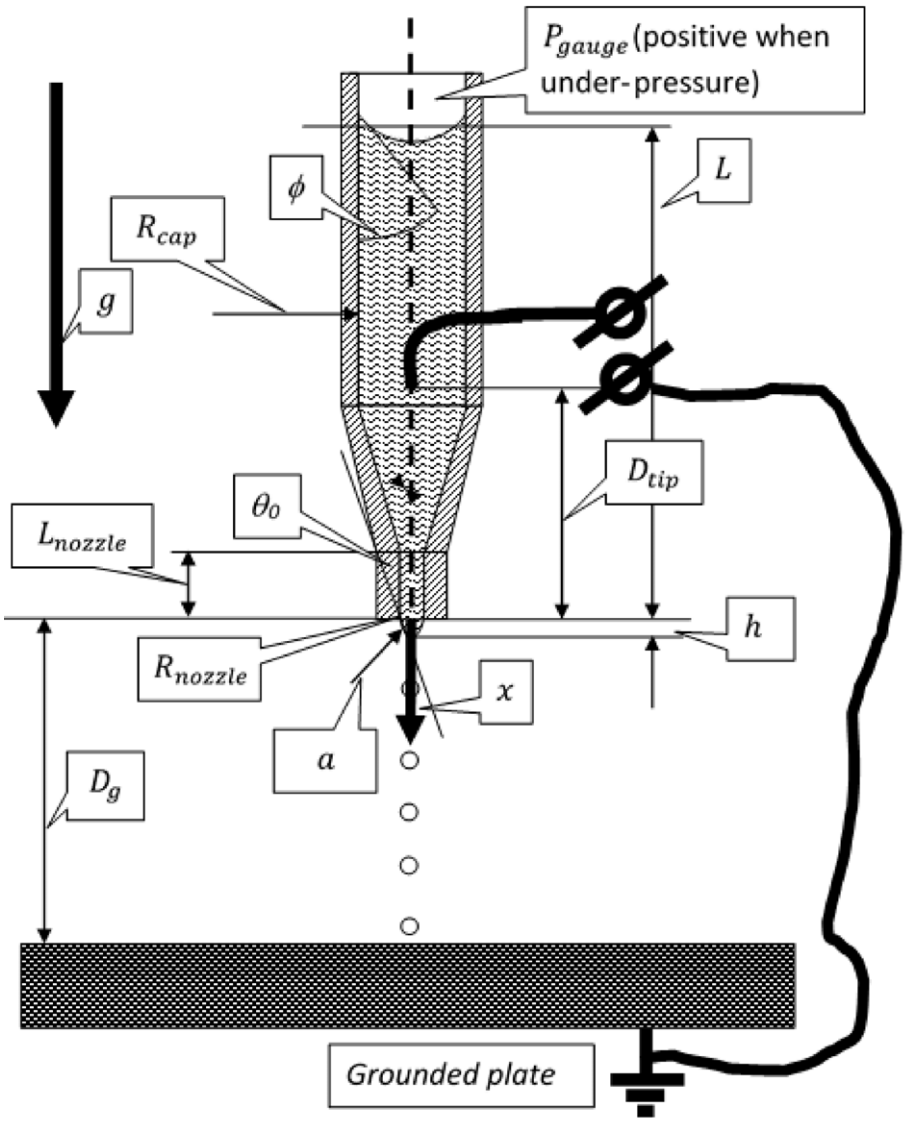

Figure 1. Geometrical details of the on-demand electrohydrodynamic jetting (Single Event Electrospraying) set-up with meniscus attached to inner rim of nozzle. Upper case symbols refer to constant values, lower case symbols vary during jetting. The fluid displacement (co-ordinate) x starts at the nozzle front and is positive downward. The schematic is based on the Autodrop AD-H-501 single nozzle glass capillary without piezo actuator from Microdrop Technologies, Norderstedt, Germany. The distance between nozzle front and the grounded plate measures $D_g = 0.8$ mm.

The fluid used is Newtonian and is a mixture of 70% ethylene glycol (Merck, purity $GC > 99.5\%$) and 30% demineralized water (percentages by volume, see [36] for material data). The properties of the fluid are presented in Table I. The conductivity of the fluid has been measured with a Meterlab IOM 450 using a 4-point probe.

On-demand electrohydrodynamic jetting starts from an equilibrium situation characterized by a fluid column of certain length supported by a pending meniscus formed at the end of a nozzle at the bottom end of a capillary and surface tension at the top of the fluid column in the capillary. The statement about surface tension high up in the capillary holds true as long as the contact angle ϕ between the liquid and the inner wall of the capillary is smaller than 90°. The equilibrium may include a gauge pressure to prevent the device from dripping during idling or to control the shape of the pending meniscus and a bias voltage.

Table I. Characteristic values of ethylene glycol (70%) and demineralized water (30%) mixture.

Parameter	Value	Units
Density ρ	1079	kg/m^3
Viscosity μ	0.0072	Pa.s
Surface tension γ	0.0554	N/m
Relative permittivity ϵ_r	56	—
Conductivity κ	2.76×10^{-4}	S/m

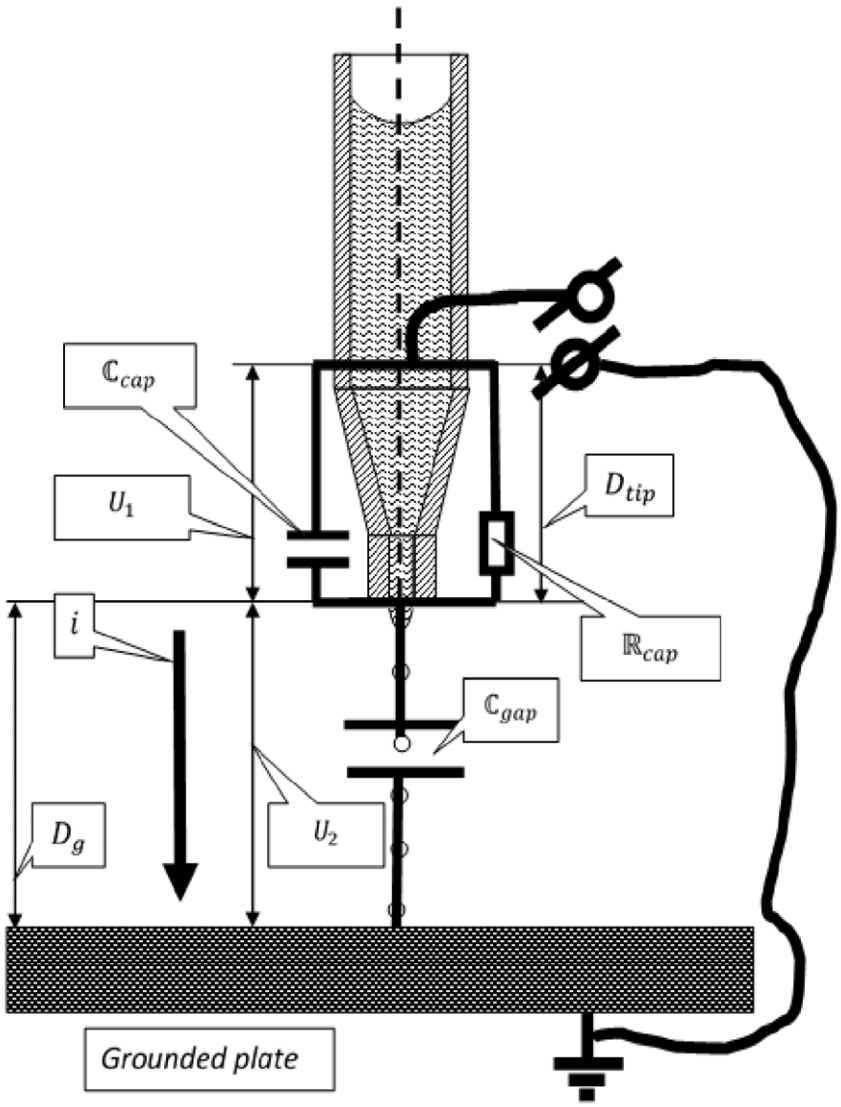

Figure 2. Components of the electrical circuit used for on-demand electrohydrodynamic jetting and definition of U_1 and U_2 and current leaving the meniscus during droplet emission i. The applied voltage is $U = U_1 + U_2$. The current i is associated with the jet leaving the meniscus and that decomposes into a stream of charged droplets flying toward the grounded plate. There is no bias voltage set. The height of the pulse is 2800 V and its duration 300 μs. The dielectric strength of air is about 3 kV/mm. For the experiments the applied voltage should remain below this value.

The meniscus is attached to the inner rim of the nozzle. To manage this the nozzle front is covered with an anti-wetting self-assembled 1H.1H.2H.2H perfluorodecyl-trichlorosilane-based monolayer [7].

By applying a pulse, an electrical field is created between the meniscus and the grounded plate and at some time after switching on the pulse, jetting starts. The jet decomposes into small droplets. Almost directly after switching off the pulse, droplet emission stops. There are no additional means to reshape the meniscus after pulsing and jetting other than hydrostatics and surface tension. All fluid motions are governed by the pressures involved: hydrostatic pressure, capillary pressure (effective capillary pressure at the pending meniscus and capillary pressure high up in the capillary) and viscous drag. From the electrical point of view, it is about electrostatics during the idle state and electrodynamics and electrokinetics during pulsing.

Fig. 3 shows a typical experimental result. In the caption, the experimental settings are given together with the volume deposited. Jetting starts after a period of hundreds of microseconds. Apparently after stopping the pulse jetting continues for a while. This is because of the limited velocity of the droplets at the moment they detach from the meniscus. As there is no electrical field anymore, they will not be accelerated and travel slowly toward the substrate.

Clearly, it is visible that initially a jet emerges from the tip of the cone. At some distance from the tip of the cone the jet decomposes into a stream of small droplets. The trajectory of the droplets stays straight and maintains its directionality. This experimental result gives an indication

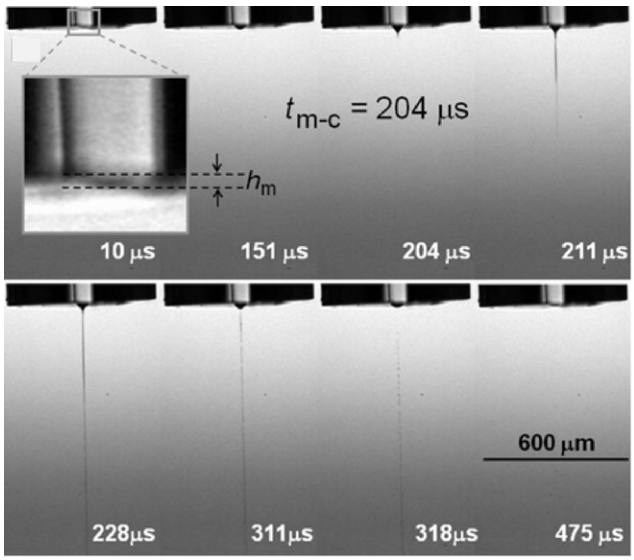

Figure 3. Series of photographs displaying different stages of a single electrospraying event from a meniscus attached to the inner rim of the nozzle (diameter 50 µm) at the end of a capillary [7]. Shown is the process of jet formation and decomposition into droplets from a capillary filled with a fluid column of 21.3 cm placed at a gap height 0.8 mm from the substrate, driven by a 2800 V pulse of 300 µs. Volume deposited ≈ 5–6 pL. Jetting starts at 204 µs from the leading edge of the pulse. Jetting frequency 1–10 Hz. Note that after switching off the pulse, droplets are visible.

what small means for the distance between the nozzle and the substrate, in this case about 1 mm.

3. STATIC EQUILIBRIUM CONSIDERATIONS IN THE NON-CHARGED AND CHARGED STATE

The radius of the nozzle is small, so small that gravity does not play any role to shape the meniscus. This can be checked by examining the capillary length [16, 37]. The capillary length κ^{-1} is defined by:

$$\kappa^{-1} = \sqrt{\frac{\gamma}{\rho g}}. \tag{1}$$

Here γ is the surface tension, ρ the density and g the earth gravitational acceleration (9.81 m/s^2). The capillary length is for common liquids of the order of magnitude of mm's. Thus for a nozzle with a radius of 25 µm and fluidic details of the same order of magnitude or smaller, the influence of gravity can be ruled out.

The effect of charging the meniscus by applying an electrical field between the meniscus and the grounded plate is that the apparent surface tension will be reduced. Surface tension results from the difference in attraction between molecules at the interface fluid/air and in the fluid. Equally charged particles on the surface repel each other. On the surface of a conductor (an equipotential surface), the lines of force are perpendicular. The tension along such a line of force meeting the conductor surface with charge density σ is given by [38] ($\epsilon = \varepsilon_0\varepsilon_r$, ε_0 being the permittivity of free space $\varepsilon_0 = 8.842 \times 10^{-12}\, F/m$ and ε_r the relative permittivity, in air $\varepsilon_r = 1$, in the ethylene glycol–water mixture $\varepsilon_r = 56$):

$$F = \frac{\sigma^2}{2\epsilon}. \tag{2}$$

Note that the charge density is measured in C/m^2 and that the unit of ϵ is $C^2/N/m^2$. Thus the unit of F is $N/m^2 = Pa$ (unit of stress, pressure). The tension does not depend on the sign of the charge. Using Young's equation, the pressure behind the meniscus is (a radius of curvature of meniscus):

$$p = \frac{2\gamma}{a} - F = \frac{2\gamma}{a} - \frac{\sigma^2}{2\epsilon}. \tag{3}$$

The effective surface tension is defined by:

$$\gamma_{\text{effective}} = \gamma\left(1 - \frac{\sigma^2 a}{4\epsilon\gamma}\right). \tag{4}$$

Charge on the meniscus will reduce the effective surface tension and consequently the capillary length. Even when the effective surface tension has been reduced with a factor of hundred, the capillary length is still much larger than the radius of the nozzle (25 µm), meaning that the shape of the blob of fluid under the nozzle is still controlled by the low effective surface tension only and will stay spherical.

Static equilibrium without electrical field means that the pressure at nozzle front in fluid column equals the capillary pressure behind the pending meniscus:

$$-P_{\text{gauge}} - \frac{2\gamma}{R_{\text{cap}}}\cos\phi + \rho g L = \frac{2\gamma}{a}. \tag{5}$$

Above the meniscus high up in the capillary, a pressure P_{gauge} is maintained to keep the fluid column in place and prevent leakage from the nozzle during idling. Also P_{gauge} can be used to control the equilibrium shape of the meniscus. The second term in the left hand side gives the surface tension pressure at the top meniscus. The third term is the hydrostatic pressure at the nozzle front coming from the fluid column in the capillary. The right hand side is the meniscus pressure at the nozzle opening.

In case an electrical field is applied, two effects must be taken into account:

- Decrease of effective surface tension.
- Attraction between the meniscus and the grounded plate of the capacitor formed by the meniscus and the grounded plate.

Following the treatise of Smythe [38], the charge density on the spherical cap loaded by a potential U is given by (the relations between variable parameters a, d and θ_0, and fixed parameters R_{nozzle} and D_g are: $a = R_{\text{nozzle}}/\sin\theta_0$, and $d = D_g + a\cos\theta_0$), see Figure 4:

$$\sigma \approx \epsilon\frac{1}{a}\left[1 + \frac{a}{2d}\frac{\left(1 + \frac{a}{2d}\right)}{\left(1 - \frac{a}{2d}\right)^2}\right]U. \tag{6}$$

The approximation holds true for $a \ll d$. The total charge on the dome surface is equal to the charge distribution (being approximately constant) times the surface area of the dome:

$$Q \approx 2\pi\epsilon a\,(1-\cos\theta_0)\left[1+\frac{a}{2d}\frac{\left(1+\frac{a}{2d}\right)}{\left(1-\frac{a}{2d}\right)^2}\right]U. \quad (7)$$

The capacitance of the capacitor formed by a spherical dome and a grounded plate is the ratio of the total charge and the applied potential:

$$C=\frac{Q}{U}=2\pi\epsilon a\left\{(1-\cos\theta_0)\left[1+\frac{a}{2d}\frac{\left(1+\frac{a}{2d}\right)}{\left(1-\frac{a}{2d}\right)^2}\right]\right\}. \quad (8)$$

The attractive force between the meniscus and the plate follows from (using the approximate formula for large gaps):

$$F=-\frac{1}{2}U^2\frac{\partial C}{\partial D_g}=-\frac{1}{2}U^2\frac{\partial C}{\partial d}\approx\frac{1}{2}\pi\epsilon\,(1-\cos\theta_0)\,\frac{a^2}{d^2}U^2. \quad (9)$$

In the charged state the equilibrium equation of pressure at the nozzle front consists of the following terms (note that the static pressure inside the pending meniscus equals the sum of the hydrostatic pressure, the gauge pressure and the capillary pressure high up in the capillary. The dimension of the pending meniscus is small compared with the fluid height in the capillary, its contribution to the hydrostatic pressure is neglected):

- Upward pressure due to reduced surface tension of meniscus:

$$\frac{2\gamma}{a}\left(1-\frac{\sigma^2}{4\epsilon\gamma}a\right)=\frac{2\gamma}{a}\left(1-\Sigma U^2\right),$$
$$\Sigma=\frac{1}{4}\frac{\epsilon}{\gamma}\frac{1}{a}\left[1+\frac{a}{2d}\frac{\left(1+\frac{a}{2d}\right)}{\left(1-\frac{a}{2d}\right)^2}\right]^2. \quad (10)$$

- Static pressure acting downward:

$$p_{\text{static}}=\left(-P_{\text{gauge}}-\frac{2\gamma}{R_{\text{cap}}}\cos\phi+\rho gL\right). \quad (11)$$

- Capacitance pressure acting downward:

$$\Phi U^2,\quad \Phi=\frac{1}{2}\frac{\epsilon\,(1-\cos\theta_0)}{R^2_{\text{nozzle}}}\frac{a^2}{d^2}. \quad (12)$$

For equilibrium in the charged state it holds:

$$\frac{2\gamma}{a}\left(1-\Sigma U^2\right)=\left(-P_{\text{gauge}}-\frac{2\gamma}{R_{\text{cap}}}\cos\Phi+\rho gL\right)+\Phi U^2. \quad (13)$$

This equation delivers an expression for the square of the applied voltage U, being the voltage across the capacitor formed by the meniscus and the grounded plate:

$$U^2=\frac{\frac{2\gamma}{a}-\left(-P_{\text{gauge}}-\frac{2\gamma}{R_{\text{cap}}}\cos\phi+\rho gL\right)}{\Phi+\frac{2\gamma}{a}\Sigma}. \quad (14)$$

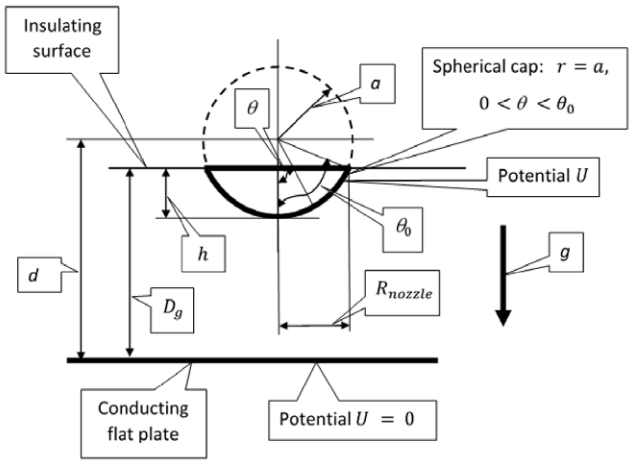

Figure 4. Spherical fluid cap filled with a conducting liquid of which the meniscus is kept at potential U.

The result is shown in Figure 5. Here the voltage U for equilibrium is given as a function of the volume displacement x defined as the ratio of the volume contained in the dome of fluid and the surface area of the nozzle:

$$x=\frac{\text{Volume dome}}{\pi R^2_{\text{nozzle}}}=\frac{1}{3}R_{\text{nozzle}}\frac{2-\cos\theta_0-\cos^2\theta_0}{\sin\theta_0\,(1+\cos\theta_0)}. \quad (15)$$

The position $x=0$ gives the situation with a flat meniscus.

For the experimental case ($L=0.213$ m), the fluid is partly contained in the Teflon tube. As Teflon is neutral-wetting, the contact angle measures $\Phi=90°$. Instead of holding up the fluid column, the meniscus inside the Teflon tube does not contribute at all to support the fluid column. In static equilibrium the height of the fluid column has pushed the meniscus at the nozzle downward over a distance of $x_{\text{equilibrium}}=3.5$ µm. At the verge of stability, the effective surface tension is still about 51% of γ. In case a bias voltage is chosen, its value must be set below the equilibrium curve. Otherwise, the liquid column cannot be kept in position.

4. EQUATION OF MOTION OF FLUID COLUMN

4.1 *Introduction*

Upon switching on the voltage across the fluid column from the tip of the electrode placed inside the capillary and the grounded plate, there are three possibilities:

- The voltage is lower than the equilibrium value. The fluid column adapts its position to the lower effective surface tension and after a while the motion of the fluid column stops. This case has been discussed in Section 3.
- The voltage is between the equilibrium value and the value at which the effective surface tension vanishes.

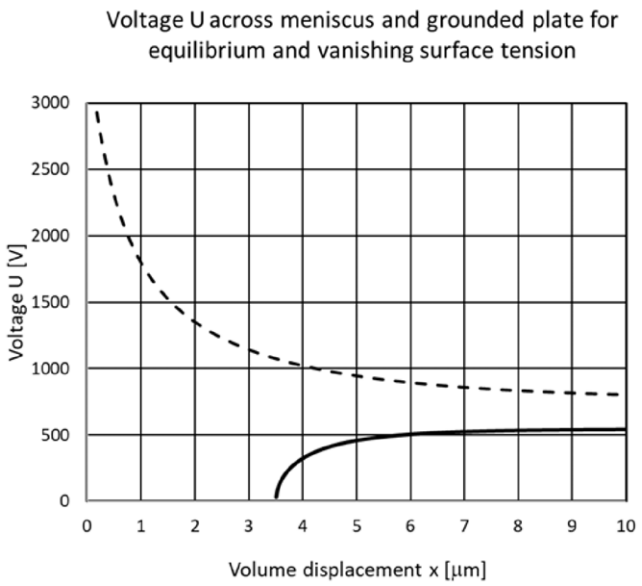

Figure 5. Equilibrium result for charged state. The no-charged starts at $x = 3.5$ μm (contact angle fluid/Teflon $\Phi = 90°$). Two lines are shown. The black continuous line give the maximum voltage at which the fluid column is just kept in position. The dashed line gives the voltage at which the surface tension completely vanishes.

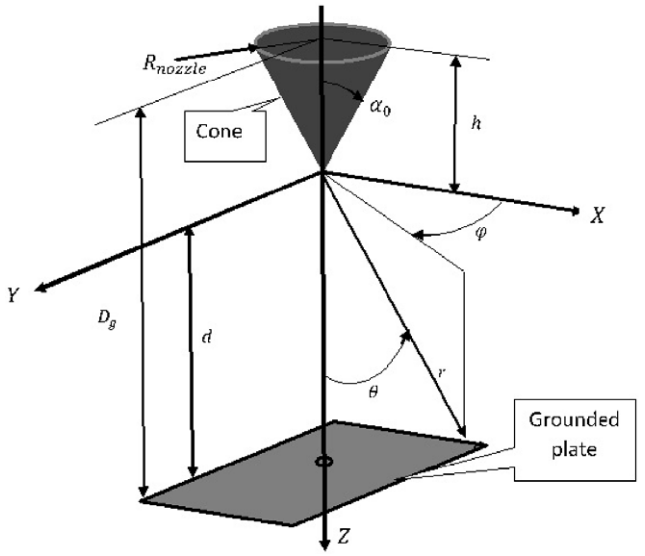

Figure 6. Geometry of a pending fluid cone of height h and base radius R_{nozzle}. Half the apex angle measures α_0. The axis of the cone is placed at right angles with respect to a grounded plate. The distance between nozzle front and plate equals D_g. The distance between tip of the cone and the grounded plate is given by $d = D_g - h$. With respect to the tip of the cone a spherical co-ordinate system (r, θ, φ) is defined.

The effective surface tension is not able to hold the fluid column in position and it starts to move downward. The meniscus grows in size, but stays spherical. At some moment in time the meniscus has become so curved that it passes the vanishing effective surface tension limit.

- The voltage is higher than the value at which the effective surface tension has become zero. The effective surface tension becomes negative generating a negative pressure behind a spherical meniscus. Such a situation is unstable and the spherical meniscus will collapse to a cone that can withstand much higher voltages than a spherical dome.

The last possibility applies to the case described in this article. The applied voltage is high, far higher than the maximum voltage a spherical fluid dome can carry. When no voltage is applied, the meniscus bulges outward in order to support the fluid column. Upon charging the spherical meniscus beyond the value at which the effective surface tension vanishes, its shape changes into a cone with the same content. The cone is depicted in Figure 6.

In the idling state, there is no charge shift in the system. Upon switching on the pulse, first of all the capacitors in the system (see Fig. 2) must be loaded. This effect takes place in a short time, so short that there is hardly any fluid displacement and we assume that the content of the meniscus does not change. The current during start-up is large and causes the fluid to start to flow with considerable velocity ("kick-start"). When the capacitors are loaded, the liquid column starts to move downward and the meniscus changes shape and consequently the capacitance of the capacitor made out of the meniscus and the grounded plate. The time rate of change of a capacitor induces an electrical current. Finally, the droplet emission starts and the current through the capillary between the tip of the electrode and the meniscus equals the charge per unit time carried away with the droplets. At the end of the pulse the field disappears almost instantaneously, generating a large current that decelerates the fluid column ("emergency stop").

Loading, unloading, adapting capacitors and generating droplets means a time rate of change of charge and consequently current. The electrical conduction in the fluid is coupled to mobile ions rather than electrons as in metals [1, 18]. The current is coupled to moving ions, more precisely to the motion of excess positively or negatively charged ions that accommodate the current considered. We postulate that the ions are generated at the electrode by electrolysis of water in the mixture, so it is about hydrogen or hydroxyl ions (H^+ and OH^-). Hydrogen ions may also be present due to the dissolution of CO_2. In other fluids, such as electrolytes, conduction is due to dissolved dissociated ions [18].

Moving charged ions cause an internal force in the fluid (body force), called the electrokinetic force defined by [18]:

$$F_{\text{electrokinetic}} = i_0 \frac{D_{\text{tip}}}{k} k = \frac{ze}{6\pi \mu a_{\text{ion}}}, \tag{16}$$

where i_0 is the current through the capillary between the tip of the electrode and the nozzle front, D_{tip} is the distance between the tip of the electrical wire in the capillary and the nozzle front and k is the mobility of the charged particles given in $m^2/V/s$. In the definition of k, ze stands for the

elementary charge e times the valency z, μ for Newtonian viscosity and a_{ion} for the hydraulic radius of the ion. The current i_0 is a measure for the number of moving ions involved. The body force acts on the whole fluid contained in the converging space between the tip of the electrode and the meniscus. Part of the force is supported by the wall of the converging space and the remaining part will be effective for the dynamics of the fluid inside the nozzle. To account for this effect, the effective electrokinetic force is defined by:

$$F_{\text{electrokinetic, eff}} = i_0 \frac{A_{\text{nozzle}}}{A_{\text{capillary}}} \frac{D_{\text{tip}}}{k} = i_0 \frac{R^2_{\text{nozzle}}}{R^2_{\text{capillary}}} \frac{D_{\text{tip}}}{k} = i_0 \frac{D_{\text{tip}}}{k_{\text{eff}}}$$

$$k_{\text{eff}} = k \frac{R^2_{\text{capillary}}}{R^2_{\text{nozzle}}}. \tag{17}$$

The mobility k is inversely proportional to the viscosity μ. The values for the mobility k of ions in water that can be looked up in text books [39]: e.g. for $H^+ k = 36.23 \times 10^{-8}$ $m^2/s/V$ and $OH^- k = 20.64 \times 10^{-8}$ $m^2/s/V$. The mixture tested contains 30% of water and the viscosity is 7.2 mPas. A guess for k that makes sense regarding the values in water and that ends up with a reasonable correspondence between the experiments and the outcomes of our calculations is $k = 5 \times 10^{-8}$ $m^2/V/s$. Using the data for the set-up, the mobility k_{eff} equals to 1.28×10^{-5} $m^2/V/s$. This value will be used in the next paragraphs. It will be shown that the electrokinetic force is important to understand the details of the on-demand electrohydrodynamic jetting method.

In order to analyze the start-up and shutting-off, characteristics of the high voltage amplifier are crucial. In the experiments reported previously by Stachewicz et al. [5], a Trek Model 5/80 has been used; the slew rate of this device is higher than 1000 V/μs. We show that the start-up with such a steep pulse gives the fluid column a "kick-start" effect and likewise for shutting off an "emergency stop" effect.

The layout of this section is as follows. We start with deriving expressions for the properties of the electrical components in the system with special attention to the capacitance of the capacitor made out of the meniscus outside the nozzle and the grounded plate (in the air). Then the "kick-start" phenomenon directly after the leading edge of the pulse will be analyzed. The results of start-up analysis will be used as an initial condition for the flow during filling of the meniscus up to the moment droplet emission starts. It is assumed that droplet emission starts when the meniscus has reached the shape of a Taylor cone [40]. After switching off the pulse in the fluid again large currents are present to remove almost instantaneously the charge from the capacitors and fluid flow is stopped abruptly. The surface tension is restored and pushes the fluid column slowly back to its equilibrium position.

4.2 *Capacitances of the On-demand Electrohydrodynamic Jetting System*

When dealing with the dynamics of on-demand electrohydrodynamic jetting (single event electrospraying), it is about changing capacitances and related shifts in charge. The time rate of change of charge means current and current means electrokinetic forcing.

As depicted in Fig. 2, the basic electrical diagram of the circuit used for electrospraying consists of a capacitor $\mathbb{C}_{\text{cap}}$ and a resistor $\mathbb{R}_{\text{cap}}$ in the capillary between the tip of the electrode and the nozzle front. In the free space (air) between the fluid meniscus and the grounded plate, there is a capacitor with capacitance $\mathbb{C}_{\text{gap}}$. The value of $\mathbb{R}_{\text{cap}}$ and $\mathbb{C}_{\text{cap}}$ follow from (series connection of infinite small resistors and capacitors with dimensions dx and πr_x^2 following the dimensions of the capillary used):

$$\mathbb{R}_{\text{cap}} = \frac{1}{\kappa} \int_0^D \frac{dx}{\pi r_x^2}, \quad \frac{1}{\mathbb{C}_{\text{cap}}} = \frac{1}{\varepsilon_0 \varepsilon_r} \int_0^{D_{\text{tip}}} \frac{dx}{\pi r_x^2}. \tag{18}$$

The conductivity of the fluid is denoted by κ, measured in S/m. Both $\mathbb{R}_{\text{cap}}$ and $\mathbb{C}_{\text{cap}}$ do not change during the operation of the device. For the set-up used, the values of the resistance and capacitance in the capillary are [5] ($\varepsilon_r = 56, \kappa = 2.7 \times 10^{-4}$ S/m):

$$\mathbb{R}_{\text{cap}} = 7.07 \times 10^8 \Omega, \quad \mathbb{C}_{\text{cap}} = 2.3 \times 10^{-15} F = 2.3 fF. \tag{19}$$

The dome case has been discussed in Section 3. For higher voltages the dome cannot carry any further the charge and changes shape to a cone. First the properties of the classic Taylor cone will be discussed ([40], see Appendix 6.1 and Fig. 6).

The total charge on the Taylor cone and its capacitance are given by (see Appendix 6.1.):

$$Q_{\text{Taylor}} = 1.878 \times 10^{-5} R_{\text{nozzle}} \sqrt{\gamma R_{\text{nozzle}}}.$$

$$\mathbb{C}_{\text{Taylor}} = \frac{Q}{U} = \frac{1.878 \times 10^{-5} R_{\text{nozzle}} \sqrt{\gamma R_{\text{nozzle}}}}{U} = 0.197 \ [fF] \quad \text{for } U = 2800V. \tag{20}$$

The capacitance force turns out to be zero.

The total charge on the Taylor cone does not depend on the applied potential and gap between nozzle and substrate. It is solely determined by the equilibrium between electrostatic tension and surface tension. This equilibrium does not induce any pressure inside the cone and does not contribute to the overall equilibrium.

In equilibrium, the spherical meniscus has moved out over a volume displacement distance $x_{\text{equilibrium}}$, which is usually much smaller than the volume displacement of the Taylor cone: $x_{\text{equilibrium}} \ll x_{\text{Taylor}}$ (for the experiment 3.5 μm ≪ 7.17 μm). Upon charging above the charge limit, the dome flips to a cone with half apex angle $\alpha > \alpha_{\text{Taylor}}$, called a pseudo-Taylor cone. Such a cone can carry much higher charges, without its shape becoming unstable.

The charge carried by the pseudo-Taylor cone and the capacitance of a pseudo-cone/flat plate arrangement read:

$$Q = 2\pi \epsilon A R_{\text{nozzle}} \left[\frac{\partial P_\nu (\cos\theta)}{\partial \theta} |_{\theta = \pi - \alpha} \right] \frac{1}{\nu + 1} \left(\frac{R_{\text{nozzle}}}{\sin \alpha} \right)^\nu$$

$$\mathbb{C}_{\text{pseudo cone}} = \frac{Q}{U}. \tag{21}$$

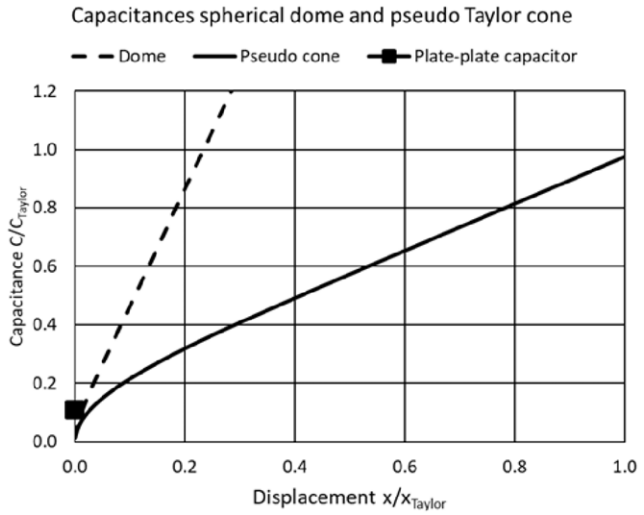

Figure 7. Capacitances of a spherical fluid dome and a fluid cone scaled with the capacitance of a Taylor cone as functions of the fluid displacement x/x_{Taylor}. For reference purposes the capacity of a parallel plate capacitor in air is given (plate radius $R_{\text{nozzle}} = 25$ μm, $D_g = 0.8$ mm. The capacitance of the pseudo-cone does not depend on the gap distance D_g. The capacitance of a parallel plate capacitor, however, does.

In Figure 7, the capacitance of the capacitor (in air) made out of the meniscus and the grounded plate is shown as a function of the fluid displacement x (content fluid outside the nozzle divided by the cross-section of the nozzle, Eq. (15)). There are two branches. The steep dashed curve represents the dome capacitance (Eq. (8)). The continuous curve shows the cone capacitance. For reference purposes, the capacitance of a plate–plate capacitor in air with area being the cross-section of the nozzle placed at a distance of 0.8 mm has been determined and equals 0.0217 fF [41]. In calculations it will be assumed that the capacitance will never be lower than the capacitance of a parallel plate capacitor. Clearly it is visible that the dome behaves differently from the cone. The dome curve is steep and therefore a dome-shaped meniscus is not able to carry a large voltage. The pseudo-Taylor cone capacitance is much less steep and is able to withstand high voltages.

An important parameter is the derivative of the capacitance $C_{\text{pseudo cone}}$ with respect to x. As can be seen in Fig. 7, the capacitance of the pseudo-Taylor cone is almost a straight line, a good approximation of the derivative is given by:

$$\frac{\partial C_{\text{pseudo cone}}}{\partial x} = \frac{C_{\text{Taylor}} - C_{\text{parallel plate}}}{x_{\text{Taylor}}}. \tag{22}$$

4.3 *Start-up of Pulse*

Upon applying the step in voltage, in a short while the meniscus changes from dome shaped to a cone. A short while can be specified as the quarter of the periodic time of the axisymmetric free oscillation of a pending meniscus. In Appendix 6.3, the analysis of the dynamics of a fluid meniscus is given. For a dome with mean displacement $x = 3.5$ μm ($\theta_0 = 0.534$ rad), the resonance frequency is 76 kHz and the periodic time 13 μs. In a quarter of the periodic time, the dome flips to an ellipsoid that in the end turns into a cone. During this time interval the capacitance of the gap capacitor changes from the dome value to the cone one. For the calculation we will use the mean value:

$$\mathbb{C}_{\text{gap}} = (\mathbb{C}_{\text{dome}} + \mathbb{C}_{\text{cone}})/2. \tag{23}$$

The dome capacitance is given by Eq. (8) and the truncated cone capacitance by Eq. (21). The electrical and hydrodynamic phenomena in the capillary and on the meniscus are governed by different time constants. The viscous time constant is defined as the ratio of the mass in the capillary and the viscous drag concentrated in the narrow part of the nozzle (M mass scaled to nozzle, K damping in nozzle region, K follows from Poiseuille's law [1] assuming the fluid is Newtonian):

$$\begin{aligned}
\tau_{\text{viscous}} &= \frac{M}{K}, \\
M &= \rho \left[A_{\text{cap}} (L - L_{\text{nozzle}}) \frac{A_{\text{nozzle}}^2}{A_{\text{cap}}^2} + A_{\text{nozzle}} L_{\text{nozzle}} \right], \\
K_{\text{viscous}} &= 8\pi \mu L_{\text{nozzle}}.
\end{aligned} \tag{24}$$

Filling in the data of the experiment $\tau_{\text{viscous}} = 19.8$ μs. This time is short with respect to the pulse time of 300 μs. The charge relaxation time constant in the capillary is defined by:

$$\tau_{\text{cap}} = \mathbb{R}_{\text{cap}} \mathbb{C}_{\text{cap}} = \frac{\varepsilon_0 \varepsilon_r}{\kappa}. \tag{25}$$

The RC time is given by:

$$\tau_{RC} = \mathbb{R}_{\text{cap}} \left(\mathbb{C}_{\text{cap}} + \mathbb{C}_{\text{gap}} \right). \tag{26}$$

The charge relaxation time constant of the capacitor made out of the meniscus and the grounded plate and the resistance in the capillary is:

$$\tau_{\text{gap}} = \mathbb{R}_{\text{cap}} \mathbb{C}_{\text{gap}}. \tag{27}$$

The values of the electrical time constants are of the order of magnitude microseconds. The slew rate of the high voltage power amplifier is described by a slew rate time constant τ_{Trek}. Based on the specifications of the amplifier, we will use $\tau_{\text{Trek}} = 1$ μs.

Using Kirchhoff's law [42] it holds (with i_0 the current though the resistor, i_1 the current toward the capacitor $\mathbb{C}_{\text{capillary}}$ and i_2 the current toward the capacitor $\mathbb{C}_{\text{gap}}$):

$$i_0 + i_1 = i_2. \tag{28}$$

With Ohm's law and the equations relating the time rate of change of capacitance and current [42]:

$$\begin{aligned}
i_0 = \frac{U_1}{\mathbb{R}_{\text{cap}}}, \; i_1 = \mathbb{C}_{\text{cap}} \frac{dU_1}{dt}, \; i_2 = U_2 \frac{d\mathbb{C}_{\text{gap}}}{dt} + \mathbb{C}_{\text{gap}} \frac{dU_2}{dt} \\
\mathbb{C}_{\text{cap}} \frac{dU_1}{dt} + \frac{U_1}{\mathbb{R}_{\text{cap}}} = U_2 \frac{d\mathbb{C}_{\text{gap}}}{dt} + \mathbb{C}_{\text{gap}} \frac{dU_2}{dt}.
\end{aligned} \tag{29}$$

During start-up, the capacitance $\mathbb{C}_{\text{gap}}$ given by Eq. (23) stays constant. The applied voltage is given by (U_0 set voltage):

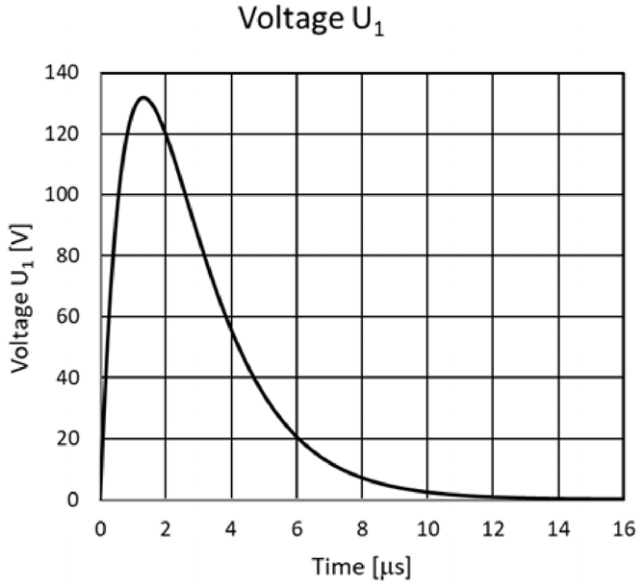

Figure 8. Voltage U_1 across the capillary between the tip of electrode and meniscus for the settings of the experiment. The slew rate time constant entered is $\tau_{\text{Trek}} = 1$ µs. The applied voltage equals 2800 V. The capacitance of the capacitor made of the meniscus and the flat grounded plate is $C_{\text{gap}} = 2.5 \times 10^{-16} F$ (mean value of pseudo-Taylor cone capacitance and the corresponding dome value, Eq. (8)).

$$U = U_0 \left(1 - e^{-\frac{t}{\tau_{\text{Trek}}}}\right). \tag{30}$$

As $U_1 + U_2 = U$, with U the applied voltage generated by the power amplifier, Eq. (29) can be rewritten as:

$$\left(\mathbb{C}_{\text{cap}} + \mathbb{C}_{\text{gap}}\right) \frac{dU_1}{dt} + \frac{U_1}{\mathbb{R}_{\text{cap}}} = \mathbb{C}_{\text{gap}} \frac{dU}{dt} = \frac{\mathbb{C}_{\text{gap}} U_0}{\tau_{\text{Trek}}} e^{-\frac{t}{\tau_{\text{Trek}}}}. \tag{31}$$

The solution is given by ($U_1(0) = 0$):

$$U_1(t) = \frac{\tau_{\text{gap}}}{\tau_{\text{Trek}} - \tau_{RC}} U_0 \left(e^{-\frac{t}{\tau_{\text{Trek}}}} - e^{-\frac{t}{\tau_{RC}}}\right). \tag{32}$$

See Figure 8 for results valid for the experimental situation. Upon substitution of the experimental data, we see that the voltage goes up to ≈130 V and then quickly drops to zero.

All motions are referred to the volume displacement in the nozzle, being defined as ratio of the volume displaced with respect to the nozzle front and the cross-section of the nozzle. During start-up, the electrokinetic force is dominant (Eq. (17)). The current through the fluid inside the nozzle and the equation of motion of the fluid inside the capillary (all forces scaled to the cross-section of the nozzle) are given by:

$$i_1(t) = \frac{U_1(t)}{\mathbb{R}_{\text{cap}}} = \frac{\tau_{\text{gap}}}{\tau_{\text{Trek}} - \tau_{RC}} \frac{U_0}{\mathbb{R}_{\text{cap}}} \left(e^{-\frac{t}{\tau_{\text{Trek}}}} - e^{-\frac{t}{\tau_{RC}}}\right)$$

$$M\dot{v} = -K_{\text{viscous}} v + i_1(t) \frac{D_{\text{tip}}}{k_{\text{eff}}} =$$

$$-K_{\text{viscous}} v + \frac{D_{\text{tip}}}{k_{\text{eff}}} \frac{\tau_{\text{gap}}}{\tau_{\text{Trek}} - \tau_{RC}} \frac{U_0}{\mathbb{R}_{\text{cap}}} \left(e^{-\frac{t}{\tau_{\text{Trek}}}} - e^{-\frac{t}{\tau_{RC}}}\right). \tag{33}$$

With solutions for the velocity of the fluid in the nozzle $v(t)$ and the corresponding fluid displacement $x(t)$ ($v(0) = 0$, $x(0) = x_0$):

$$v(t) = \frac{D_{\text{tip}}}{k_{\text{eff}}} \frac{\tau_{\text{gap}}}{\tau_{\text{Trek}} - \tau_{RC}} \frac{U_0}{K\mathbb{R}_{\text{cap}}} \left[-\left(\frac{\tau_{\text{Trek}}}{\tau_{\text{Trek}} - \tau_{\text{viscous}}} - \frac{\tau_{RC}}{\tau_{RC} - \tau_{\text{viscous}}}\right) e^{-\frac{t}{\tau_{\text{viscous}}}} + \frac{\tau_{\text{Trek}}}{\tau_{\text{Trek}} - \tau_{\text{viscous}}} e^{-\frac{t}{\tau_{\text{Trek}}}} - \frac{\tau_{RC}}{\tau_{RC} - \tau_{\text{viscous}}} e^{-\frac{t}{\tau_{RC}}} \right] \tag{34}$$

$$x(t) = \frac{D_{\text{tip}}}{k_{\text{eff}}} \frac{\tau_{\text{gap}}}{\tau_{\text{Trek}} - \tau_{RC}} \frac{U_0}{K\mathbb{R}_{\text{cap}}} \left[\tau_{\text{viscous}} \left(\frac{\tau_{\text{Trek}}}{\tau_{\text{Trek}} - \tau_{\text{viscous}}} - \frac{\tau_{RC}}{\tau_{RC} - \tau_{\text{viscous}}}\right) e^{-\frac{t}{\tau_{\text{viscous}}}} - \frac{{\tau_{\text{Trek}}}^2}{\tau_{\text{Trek}} - \tau_{\text{viscous}}} e^{-\frac{t}{\tau_{\text{Trek}}}} + \frac{{\tau_{RC}}^2}{\tau_{RC} - \tau_{\text{viscous}}} e^{-\frac{t}{\tau_{RC}}} + \tau_{\text{Trek}} - \tau_{RC} \right] + x_0.$$

The result is shown in Figure 9.

After say 6 µ s, the velocity reaches a maximum. At that moment in time, the voltage has dropped to almost zero. This maximum velocity v_0 and corresponding displacement x_0 will be used as initial conditions for the next section.

The initial filling of the capacitors in the system causes a "kick-start" to the fluid in the nozzle. This kick-start effect depends on the capacitance of the capacitor formed by the meniscus and the grounded plate. The gap capacitance depends on the curvature of the meniscus. The more curved the meniscus, the higher the gap capacitance and the larger the "kick-start" effect.

4.4 *Filling of the Meniscus*

The applied voltage is so high that the spherical dome flips to a cone. With respect to the pulse time of several 100 µs, there is an instant charge communication between the tip of the electrode and the meniscus (all electric time constants are of the order of magnitude µs's). The influence of the capacitor in the capillary can be ruled out, as its value does not change during operation. As U_1 has to start at almost zero (from the kick-start result), initially $U_1 \ll U$. This simplifies Kirchhoff's law to:

$$i_0 = i_2, \frac{U_1}{\mathbb{R}_{\text{cap}}} = U_0 \frac{dC_{\text{cone}}}{dt}. \tag{35}$$

The conduction in the fluid is coupled to mobile ions rather than electrons as in metals. As soon as there is an ionic current flowing through the fluid inside the capillary, an electrokinetic force is generated given by Eq. (16):

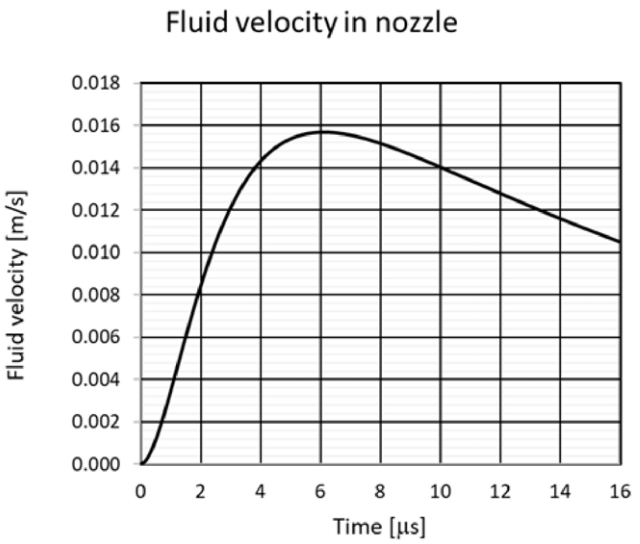

Figure 9. Fluid velocity in the nozzle. The distance between the tip of electrode and meniscus measures $D_{\text{tip}} = 1.6$ mm. For the ion mobility we have used: $k_{\text{eff}} = 1.28 \times 10^{-5}$ m^2/V/s.

$$F_{\text{cone}} = \frac{i_0 D_{\text{tip}}}{k_{\text{eff}}} = U_0 \frac{dC_{\text{cone}}}{dt}\frac{D_{\text{tip}}}{k_{\text{eff}}} = U_0 \frac{dC_{\text{cone}}}{dx}\frac{D_{\text{tip}}}{k_{\text{eff}}}\frac{dx}{dt} = U_0 \frac{dC_{\text{cone}}}{dx}\frac{D_{\text{tip}}}{k_{\text{eff}}} v = K_{\text{cone}} v. \quad (36)$$

In this section, we let the time run from the moment that during start-up the velocity has gone through a maximum and the voltage has dropped almost to zero.

To continue, it is supposed that the fluid is incompressible. Effects of traveling waves, initiated by steep pulse shapes, in the capillary will be neglected [43]. In order to derive the equation of motion of the fluid column contained in the capillary, the following short scripts are used (the inertia effects in the capillary above the nozzle are scaled to the nozzle):

$$M = \rho \left[\pi R_{\text{cap}}^2 \left(L - L_{\text{nozzle}}\right) \frac{\left(\pi R_{\text{nozzle}}^2\right)^2}{\left(\pi R_{\text{cap}}^2\right)^2} + \pi R_{\text{nozzle}}^2 L_{\text{nozzle}} \right],$$
$$K_{\text{viscous}} = 8\pi\ \mu L_{\text{nozzle}},$$
$$F_{\text{static}} = \left(-\frac{2\gamma}{R_{\text{capillary}}} \cos\Phi - P_{\text{gauge}} + \rho g L \right) \pi R_{\text{nozzle}}^2. \quad (37)$$

Viscous drag is significant only in the nozzle. The equation of motion of the fluid contained in the capillary reads:

$$M\dot{v} = -K_{\text{viscous}} v + F_{\text{cone}} + F_{\text{static}} = \left(-K_{\text{viscous}} + K_{\text{cone}}\right) v + F_{\text{static}}. \quad (38)$$

The solution of this first-order non-homogeneous linear differential equation is given by (with $v\,(0) = v_0$, $x\,(0) = x_0$, v_0 and x_0 are the results of the start-up calculation):

$$v\,(t) = \left(v_0 - v_{part}\right) e^{\lambda t} + v_{part} = v_0 e^{\lambda t} + v_{part}\left(1 - e^{\lambda t}\right)$$
$$x\,(t) = \frac{1}{\lambda}\left(v_0 - v_{part}\right)\left(e^{\lambda t} - 1\right) + v_{part}\, t + x_0$$
$$\lambda = \frac{\left(-K_{\text{viscous}} + K_{\text{cone}}\right)}{M},\ v_{part} = -\frac{F_{\text{static}}}{\left(-K_{\text{viscous}} + K_{\text{cone}}\right)}. \quad (39)$$

This solution is valid as long as the volume associated with the volume displacement x has not reached the volume of the Taylor cone (for the experiments $x = 7.17$ μm). As will be explained in the next section, this will the instant droplet formation starts.

Calculating the values of the different K's:

$$K_{\text{viscous}} = 2.17 \times 10^{-4} \frac{kg}{m},\ K_{\text{cone}} = 8.57 \times 10^{-6} \left[\frac{kg}{m}\right]. \quad (40)$$

The electrokinetic forcing term is much smaller (≈5%). The driving force during the filling of the meniscus comes from the static force. This means that the velocity strives to a constant value for large t:

$$v\,(t \to \infty) = -\frac{F_{\text{static}}}{\left(-K_{\text{viscous}} + K_{\text{cone}}\right)} \approx \frac{F_{\text{static}}}{K_{\text{viscous}}}$$
$$\text{Experimental situation: } v\,(t \to \infty) = 0.0212 \frac{m}{s},$$
$$\tau_{\text{filling}} = -\frac{1}{\lambda} = 20.6\ \mu s. \quad (41)$$

The filling time constant is smaller than the pulse time, so the stationary value of the velocity will be reached within the time window of the pulse. As the electrokinetic forcing is small, viscous drag is dominant and the fluid velocity will become a constant. The displacement, however, increases indefinitely.

4.5 *Equation of Motion of Fluid Column with Droplet Emission*

At the moment the pseudo-Taylor cone has reached the shape of a Taylor cone, a jet with radius R_{jet} starts to emerge from the tip of the cone, dragging along with it charge. The amount of charge dragged along with the jet is supposed to be the charge density at the transition zone of cone to the jet (see for specifics of the Taylor cone Appendix 6.1):

$$\sigma_{\text{jet}} = \xi \epsilon A \sqrt{\frac{\sin\alpha_{\text{Taylor}}}{R_{\text{jet}}}} \frac{\partial P_{\frac{1}{2}}\left(\cos\theta\right)}{\partial\theta}|_{\theta=\theta_0}. \quad (42)$$

The constant ξ gives the fraction of the charge density actually transferred to jet from the cone surface [2, 35]. Throughout this section, we take $\xi = 0.6$. The charge distribution is assumed to be uniform over the surface of the jet. At some moment in time, the jet breaks up into droplets, like as it happens in the dripping faucet experiment [44–47]. The force exerted by the charge on the surface of the jet between the detachment of the cone and the break-up point can easily be found by considering the integration of projected force components on the surface area of the jet:

$$F_{\text{charge}} = \frac{1}{2}\frac{\sigma_{\text{jet}}^2}{\epsilon}\pi R_{\text{jet}}^2 = \frac{1}{2}\pi\epsilon \sin\alpha_0 \xi^2 A^2 \left(\frac{\partial P_{\frac{1}{2}}(\cos\theta)}{\partial\theta}|_{\theta=\theta_0}\right)^2 R_{\text{jet}}. \quad (43)$$

Substituting the known values for all constants, it appears that F_{charge} depends on the surface tension γ, the charge transfer coefficient ξ and the radius of the jet R_{jet}:

$$F_{\text{charge}} = 2.05\xi^2\gamma R_{\text{jet}}. \quad (44)$$

In the cone sink flow is assumed. Sink flow is characterized by the fact that all velocity vectors are directed toward one point, the sink. The sink will be the origin of a spherical co-ordinate system (r, α, φ); see Fig. 6. Along the surface of the cone there is no friction; therefore, it is reasonable to suppose that the velocity does not depend on α and φ, it is only a function of r. As the volume rate of flow through the cone is constant, the velocity $v_r(r)$ is given by:

$$v_r = -\frac{v\pi R_{\text{nozzle}}^2}{2\pi r^2 (1-\cos\alpha_0)} = -\frac{1}{2}\frac{R_{\text{nozzle}}^2}{r^2(1-\cos\alpha_0)}v. \quad (45)$$

From the equation of motion for a Newtonian fluid with constant density and viscosity [48], it can be concluded that for the sink flow kinematics the pressure gradient equals zero. The deviatoric stresses at entrance and exit are:

$$\tau_{rr}|_{\text{exit}} = 2\,\mu R_{\text{nozzle}}^2 \frac{\sin^3\alpha_0}{(1-\cos\alpha_0)}\frac{1}{R_{\text{jet}}^3}v,$$
$$\tau_{rr}|_{\text{entrance}} = 2\,\mu R_{\text{nozzle}}^2 \frac{\sin^3\alpha_0}{(1-\cos\alpha_0)}\frac{1}{R_{\text{nozzle}}^3}v. \quad (46)$$

At the entrance, the elongational stress loads the fluid inside the nozzle and opposes its motion ($R_{\text{jet}} \ll R_{\text{nozzle}}$):

$$F_{\text{cone,nozzle}} = 2\pi\,\mu R_{\text{nozzle}}^2 \frac{\sin^3\alpha_0}{(1-\cos\alpha_0)}\frac{1}{R_{\text{nozzle}}}v = K_{\text{elongation}}v. \quad (47)$$

The sink flow opposes the flow through the nozzle; its influence, however, is much smaller than the effect of the viscous drag in the nozzle and will be neglected in the following. The force equilibrium is obtained through the stretching at the end of the cone. Integration of the stress component in z-direction over the cross-section at the transition of cone to jet delivers the elongational force:

$$F_{\text{elongation}} = \tau_{rr}|_{\text{exit}}\pi R_{\text{jet}}^2 = 2\pi\mu R_{\text{nozzle}}^2 \frac{\sin^3\alpha_0}{(1-\cos\alpha_0)}\frac{1}{R_{\text{jet}}}v. \quad (48)$$

The charge force pulls the jet out of the cone. Equating the charge force F_{charge} and the elongational force $F_{\text{elongation}}$ delivers an equation for the radius of the jet R_{jet}:

$$R_{\text{jet}}^2 = 2\pi\frac{\mu}{\gamma}\frac{R_{\text{nozzle}}^2}{2.05\xi^2}\frac{\sin^3\alpha_0}{(1-\cos\alpha_0)}v = C_{\text{jet}}\frac{1}{\xi^2}\pi R_{\text{nozzle}}^2 v. \quad (49)$$

Reworking gives:

$$C_{\text{jet}} = 2\frac{\mu}{\gamma}\frac{1}{2.05}\frac{\sin^3\alpha_0}{(1-\cos\alpha_0)} = 1.222\frac{\mu}{\gamma},$$
$$R_{\text{jet}} = \frac{R_{\text{nozzle}}}{\xi}\sqrt{\pi v C_{\text{jet}}} = 1.959\frac{R_{\text{nozzle}}}{\xi}\sqrt{\frac{\mu}{\gamma}v}. \quad (50)$$

This result leads to the conclusion that the jet velocity at the position the jet leaves the cone is a constant:

$$v_{\text{jet}} = \frac{R_{\text{nozzle}}^2}{R_{\text{jet}}^2}v = \frac{\xi^2}{\pi C_{\text{jet}}} = \frac{\xi^2}{\pi 1.222}\frac{\gamma}{\mu} = 0.2605\xi^2\frac{\gamma}{\mu}. \quad (51)$$

For the experiments referred to and $\xi = 0.6$, $v_{\text{jet}} = 0.722$ m/s. To be added to the description of the electrical scheme is the current i associated with the stream of droplets. The capacitance of the cone does not change anymore. Still the voltage $U_1 \ll U_{\text{Taylor}}$, so the relation of Kirchhoffs and Ohm's law become:

$$i_0 = \frac{U_1}{\mathbb{R}_{\text{cap}}},\ i_1 = 0,\ i_2 = 0,\ i_0 = i. \quad (52)$$

The current associated with the charge carried away with the jet follows from:

$$i = \sigma 2\pi R_{\text{jet}} v_{\text{jet}} = 2\pi\xi\epsilon A\sqrt{R_{\text{jet}}}\sqrt{\sin\alpha_0}\frac{\partial P_{\frac{1}{2}}(\cos\theta)}{\partial\theta}|_{\theta=\theta_0}v_{\text{jet}}. \quad (53)$$

With the values of the known constants substituted:

$$i = 2.135\times10^{-5}\xi\sqrt{\gamma R_{\text{jet}}}v_{\text{jet}}. \quad (54)$$

In the current expression, the radius of the jet and the jet velocity can be eliminated:

$$i = \left(2.988\times10^{-5}v_{\text{jet}}\sqrt{\xi\gamma R_{\text{nozzle}}\sqrt{\frac{\mu}{\gamma}}}\right)v^{1/4} = Iv^{1/4}. \quad (55)$$

The equation of motion becomes:

$$M\dot{v} = -Kv + \frac{D_g}{k_{\text{eff}}}Iv^{1/4} + F_{\text{static}}. \quad (56)$$

The initial conditions for this equation follow from the final state of meniscus filling. Numerical integration gives the velocity as a function of time. Integration once again gives the fluid displacement in the nozzle (at $t = 0$, $x = x_0$).

Returning to Eq. (56), the influence of the static load can be calculated. By substitution of $v^* = v^{1/4}$, the right hand side of the equation of motion 4–41 turns into a fourth-order algebraic equation in v^* of which solutions can be found by standard means [43]. The only relevant solution returns:

$$v\,(t\to\infty) = 0.0229\ \text{m/s}. \quad (57)$$

In Figure 10, the results of the different calculations are given.

During start-up, the "kick-start" effect is clearly visible. In 6 µs, the velocity in the nozzle has reached a value of 0.0157 m/s. The limiting value for the filling, $v\,(t\to\infty) =$

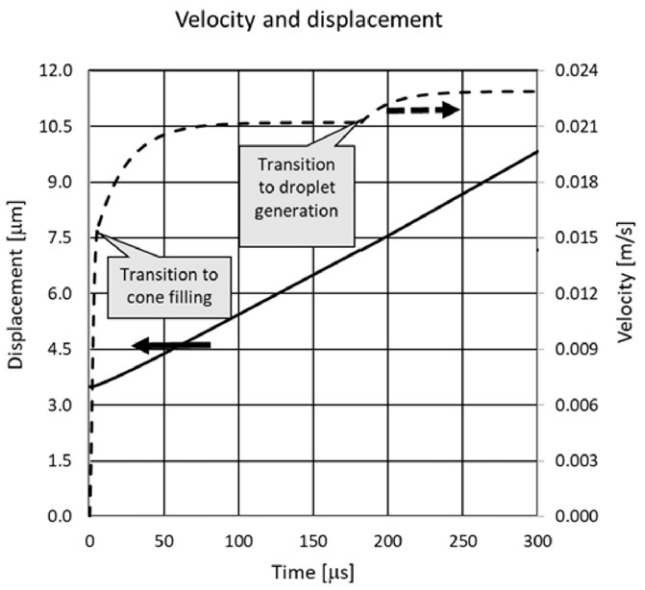

Figure 10. Fluid displacement and velocity in the nozzle of the capillary containing the fluid column of 21.3 cm. Ion mobility entered: $k_{\text{eff}} = 1.28 \times 10^{-5} \text{m}^2/\text{V/s}$ and for $D_{\text{tip}} = 1.6$ mm. Combined are the solution of the start-up phase (Section 4.3), followed by the filling according to the pseudo-cone theory (Section 4.4) followed by the results of the solution with droplet emission. The start-up phase lasts 6 µs. The droplet emission starts at $x = 7.17$ µm and $t = 182$ µs. At the end of the pulse at $t = 300$ µs the emitted volume equals 5.24 pL. The jet radius starts at 4.29 µm and grows to 4.45 µm. The jet velocity at the transition cone to jet is constant and equals 0.722 m/s. The current and voltage drop across the capillary during jetting are $i \approx 4.5 \times 10^{-9}$A, $U_1 \approx 3.2$ V, respectively. The voltage drop across the resistor is much smaller than the applied voltage of 2800 V.

0.0212 m/s, is larger than the start-up velocity. As the time constant for the filling $\tau_{\text{filling}} = 20$ µs, the limiting velocity is quickly reached even within the pulse time. The limiting velocity for the jetting case (Eq. (57)) is larger than the limiting velocity during filling because of the extra electrokinetic forcing due to the current of the charged droplets leaving the Taylor cone. The velocity goes to a constant value, the displacement increases indefinitely with time. In that respect, electrohydrodynamic jetting is a run-away process.

The picture described so far for on-demand electrohydrodynamic jetting as depicted in Fig. 3 describes in detail what has been found experimentally. It takes indeed a long time, about 200µs, for the process to start with jetting, at the moment the pulse has switched off, the volume deposited equals 5.24 pL (experimentally 5–6 pL).

4.6 *Shutting off Pulse*

During shutting off charge is removed from the meniscus and its surface tension is restored. The shape changes from the Taylor cone to a dome with the same content. As explained for the "kick-start," the capacitance used to analyze the electrodynamics and the hydrodynamics of switching off the mean value of the capacitances of the Taylor cone and a dome with equal volume will be used:

$$\mathbb{C}_{\text{cap}} = \frac{\mathbb{C}_{\text{Taylor}} + \mathbb{C}_{\text{dome}}}{2}. \tag{58}$$

The Taylor cone capacitance is given by Eq. (20) ($\mathbb{C}_{\text{Taylor}} = 0.197fF$), the equal volume dome capacitance equals $\mathbb{C}_{\text{dome}} = 0.745fF$.

Shutting off means adding a negative step in voltage to the system (for the analysis t starts at the trailing edge of the pulse):

$$\text{for } t > 0\text{: } U\,(t) = U_0 - U_0\left(1 - e^{-\frac{t}{\tau_{\text{Trek}}}}\right) = U_0 e^{-\frac{t}{\tau_{\text{Trek}}}}. \tag{59}$$

The potential decays exponentially. The effect of such a negative potential step on the dynamics of the fluid column follows the same reasoning as used for the start-up (see Section 4.3). As we have explained in Section 4.3, switching on has a strong effect on the dynamics of the fluid column, so it is reasonable to suppose that jetting stops immediately. No current is leaving the meniscus anymore. Returning to Kirchhoff's law and Ohms law:

$$\begin{aligned} &i_0 = \frac{U_1}{\mathbb{R}_{\text{cap}}},\ i_1 = \mathbb{C}_{\text{cap}}\frac{dU_1}{dt},\ i_2 = U_2\frac{d\mathbb{C}_{\text{gap}}}{dt} + \mathbb{C}_{\text{gap}}\frac{dU_2}{dt}, \\ &\mathbb{C}_{\text{cap}}\frac{dU_1}{dt} + \frac{U_1}{\mathbb{R}_{\text{cap}}} = U_2\frac{d\mathbb{C}_{\text{gap}}}{dt} + \mathbb{C}_{\text{gap}}\frac{dU_2}{dt}. \end{aligned} \tag{60}$$

It is assumed that during shutting off the capacitance $\mathbb{C}_{\text{gap}}$ (Eq. (58)) stays constant. With $U_1 + U_2 = U$:

$$\begin{aligned} U_1 + U_2 = U &= U_0 e^{-\frac{t}{\tau_{\text{Trek}}}}\left(\mathbb{C}_{\text{cap}} + \mathbb{C}_{\text{gap}}\right), \\ \frac{dU_1}{dt} + \frac{U_1}{\mathbb{R}_{\text{cap}}} = \mathbb{C}_{\text{gap}}\frac{dU\,(t)}{dt} &= -\frac{\mathbb{C}_{\text{gap}}U_0}{\tau_{\text{Trek}}}e^{-\frac{t}{\tau_{\text{Trek}}}}. \end{aligned} \tag{61}$$

The solution is given by ($U_1\,(0) = i(t_{\text{pulse}})R_{\text{cap}}$, the current belonging to jetting at the end of the pulse):

$$\begin{aligned} U_1\,(t) &= U_1\,(0)\,e^{-\frac{t}{\tau_{RC}}} - \frac{\tau_{\text{gap}}}{\tau_{\text{Trek}} - \tau_{RC}}U_0\left(e^{-\frac{t}{\tau_{\text{Trek}}}} - e^{-\frac{t}{\tau_{RC}}}\right) \\ i_1\,(t) &= \frac{U_1\,(0)}{\mathbb{R}_{\text{cap}}}e^{-\frac{t}{\tau_{RC}}} - \frac{\tau_{\text{gap}}}{\tau_{\text{Trek}} - \tau_{RC}}\frac{U_0}{\mathbb{R}_{\text{cap}}}\left(e^{-\frac{t}{\tau_{\text{Trek}}}} - e^{-\frac{t}{\tau_{RC}}}\right). \end{aligned} \tag{62}$$

The voltage as a function of time measured after the trailing edge is given in Figure 11.

The equation of motion of the fluid inside the capillary (all forces scaled to the cross-section of the nozzle) is given by:

$$M\dot{v} = -K_{\text{viscous}}v + i_1\,(t)\,\frac{D_{\text{tip}}}{k_{\text{eff}}} + F_{\text{static}} - 2\gamma\,\frac{\sin\theta_0}{R_{\text{nozzle}}}\pi R_{\text{nozzle}}^2. \tag{63}$$

The fluid displacement x as a function θ_0 is given by Eq. (15). With high precision, the inverse function namely the angle θ_0

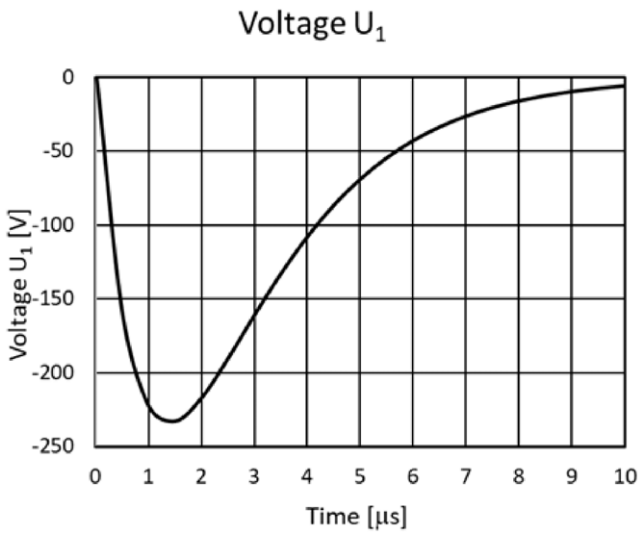

Figure 11. Voltage as a function of time. As the capacitance of the capacitor Taylor cone and grounded plate is much larger than the capacitance of the gap at the beginning of the pulse, the voltage change is much larger compared to the start-up result (see Fig. 8).

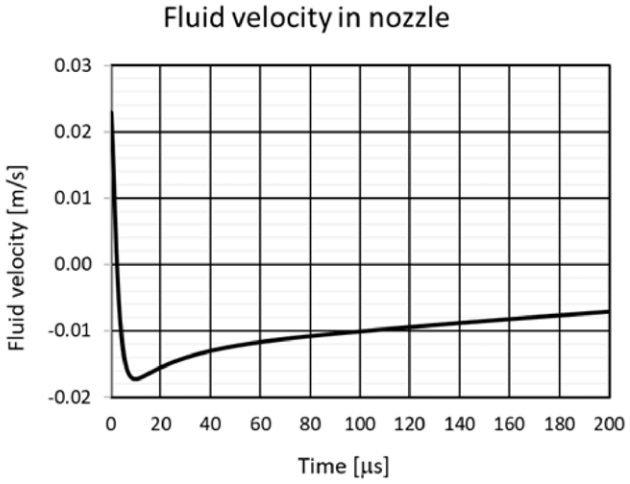

Figure 12. Velocity in the nozzle as a function of time measured from the trailing edge of the pulse. The initial velocity equals the velocity of the end of the jetting case.

as a function of x can be found by curve fitting:

$$\theta_0 = -0.9308\left(\frac{x}{R_{\text{nozzle}}}\right)^3 - 2.627\left(\frac{x}{R_{\text{nozzle}}}\right)^2 + 4.2218\frac{x}{R_{\text{nozzle}}} - 4.291\times 10^{-3}. \quad (64)$$

The equation of motion is non-linear because of the dependence of θ_0 on x, its solution is found by numerical integration starting from the initial conditions $v(0) = v(t_{\text{pulse}})$, $x(0) = x(t_{\text{pulse}})$ ($v(t_{\text{pulse}})$ and $x(t_{\text{pulse}})$ are the velocity and displacement in the nozzle at the end of the pulse, respectively) (see Fig. 10).

As shown in Figure 12, the braking effect of the switching-off effect is strong, due to the electrokinetic forcing. It looks like

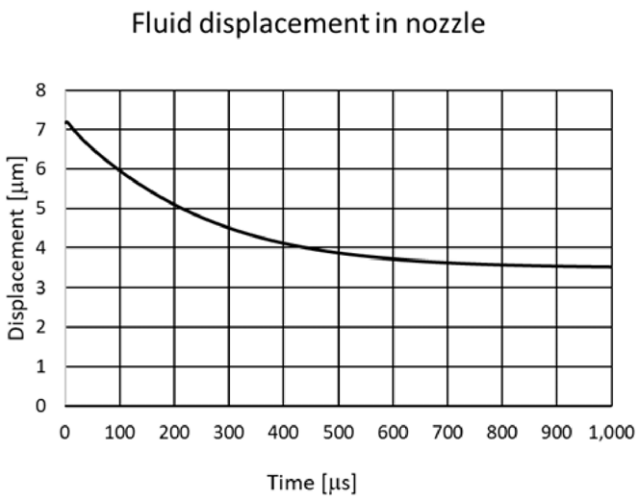

Figure 13. Fluid displacement in the nozzle as a function of time after switching off the pulse. The time is measured from the leading edge of the pulse.

an "emergency stop." Almost immediately the velocity goes to zero and becomes negative. The voltage goes equally fast to zero as depicted Fig. 11. After say 10 µs, the voltage has disappeared completely as well as the electrokinetic force. The driving force during returning to equilibrium is the surface tension and is counter-acted by the static force and viscous drag. In Appendix 6.3, the equations governing the oscillations of a fluid column supported by a surface tension spring has been derived. It appears that this system is strongly overdamped and takes a long time to return to equilibrium as depicted in Figure 13.

The time window used in Fig. 13 is much larger than the pulse time applied. After 1.3 ms (pulse time plus damping time), the meniscus has returned to its original position. As this vibrational system is strongly overdamped, the repeat rate of on-demand electrohydrodynamic jetting is limited to 0.77 kHz.

4.7 *Results and Discussion*

In Figure 14, in a large time window the overall result of the previous calculations is shown, from the kick-off start directly after the leading edge of the pulse up to returning to the equilibrium position a long time after the trailing edge. As the velocity becomes constant during jetting, it can be concluded that the volume deposited is proportional to the jetting time. The longer the pulse, the longer the jetting time and the larger the volume jetted.

We also considered the effect of the length of the fluid column above the nozzle on the performance of on-demand electrohydrodynamic jetting. The results of these calculations are listed in Table II, which shows different fluid lengths. A shorter fluid column means a reduced static pressure head and a reduced driving during cone filling, and therefore an extended cone filling time. To compensate for the loss of volume deposited, the pulse time has been taken

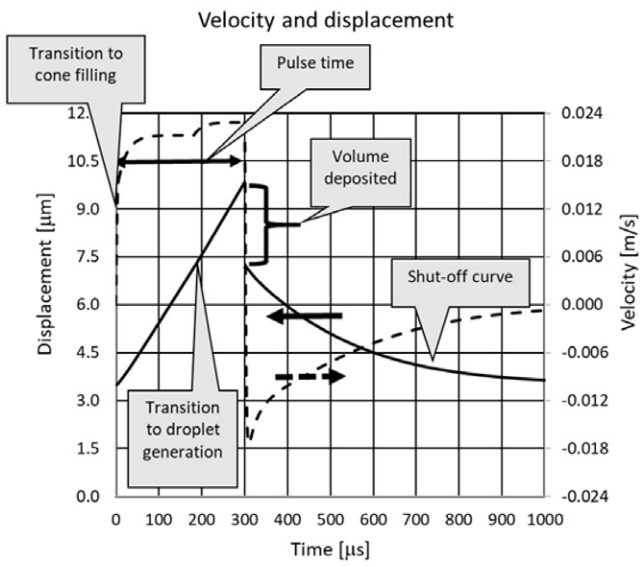

Figure 14. Total overview of fluid velocity and displacement in the nozzle during on-demand electrohydrodynamic jetting. The process starts with a kick-start at the leading edge of the pulse followed by a gradual increase of the velocity and displacement during filling of the pseudo-cone until jetting starts. After switching off, the velocity quickly goes to zero and even becomes negative starting the slow process of returning to equilibrium. The jetted volume is 5.24 pL.

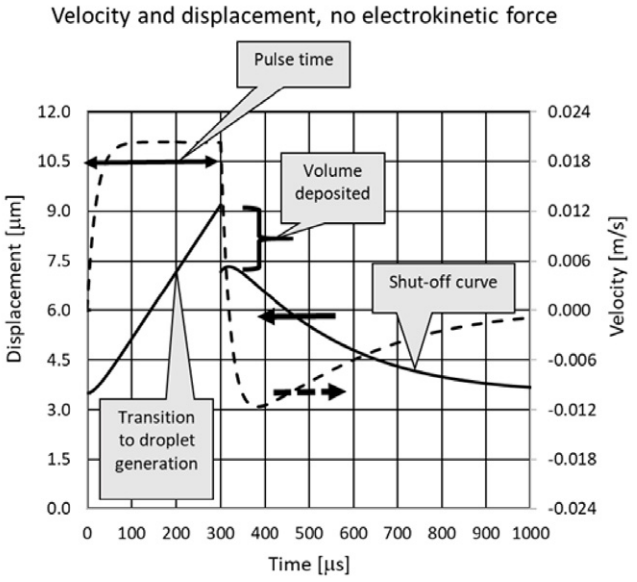

Figure 15. Overview of the results of the calculations without electrokinetic forcing. There is no kick-start effect. The transition from cone filling to jetting takes place at $t = 200$ μs. The difference between displacement during cone filling up to the end of the pulse and the displacement during shutting off is the volume deposited. In this case 4 pL.

Table II. Data showing the experimental settings and results for the various fluid column lengths.

Length fluid column [cm]	Pulse time [μs]	Cone filling time [μs]	Volume deposited [pl]
21.3	300	182	5.24
20	300	205	3.97
17.5	300	258	1.52
17.5	400	258	5.28
15	400	328	2.3
15	500	328	5.58
12.5	500	426	2
12.5	600	426	4.8

longer. The height of the pulse stays 2800 V and all other geometrical and fluid details are kept the same.

The influence of the height of the pulse is predicted to be small. The height of the pulse must be above the value at which the apparent surface tension vanishes (see Figure 5). During the filling of the cone, electrostatics do not play a role, it is the static pressure head that drives the fluid flow. During jetting, the voltage drop across the liquid is only a few volts, so here also a minor effect is expected of the height of the pulse. In our calculations, we can take the height of the pulse as low as 2000 V observing minor changes in the results.

Importantly, we checked the importance of electrokinetic forcing. Leaving out the effect of the electrokinetic forcing leads to the result shown in Figure 15. Although the overall picture looks similar, there are distinct differences. First of all, neglecting the electrokinetic forcing skips the "kick start" and "emergency stop." Secondly the volume deposited is about 30% less. This is because of the fact that the fluid velocity in the nozzle during jetting is smaller compared to the case with electrokinetic forcing. It clearly indicates that on-demand electrohydrodynamic jetting can be delivered from metal nozzles as well.

We finally discuss what happens with an almost insulating ink. We repeated the calculation with a fluid of which the resistance between the tip of the electrode and the meniscus turns out to be $\mathbb{R}_{cap} = 7.07 \times 10^{10}\Omega$ (hundred times the resistance used earlier). The results of the start calculation, the filling of the cone and jet formation and the shut-off analysis are shown in Figure 16. Roughly the picture has not changed much. But because of the much higher resistance, the electrical time constants have changed and the start-up phase takes much longer. Therefore, the time needed to fill the cone and jetting is shorter and consequently the volume deposited is less. The theory predicts that it is possible to electrospray with high resistance fluids. As the jetting does not depend on the applied voltage, the current needed to form the jet does not depend on the applied voltage as well. In case the resistance of the fluid increases further, the voltage drop in the nozzle becomes so large that the applied voltage is not able anymore to pass the vanishing surface tension limit (see Fig. 5).

5. CONCLUSIONS

On-demand electrohydrodynamic jetting, described also as Single Event Electrospraying (SEE), without external flow

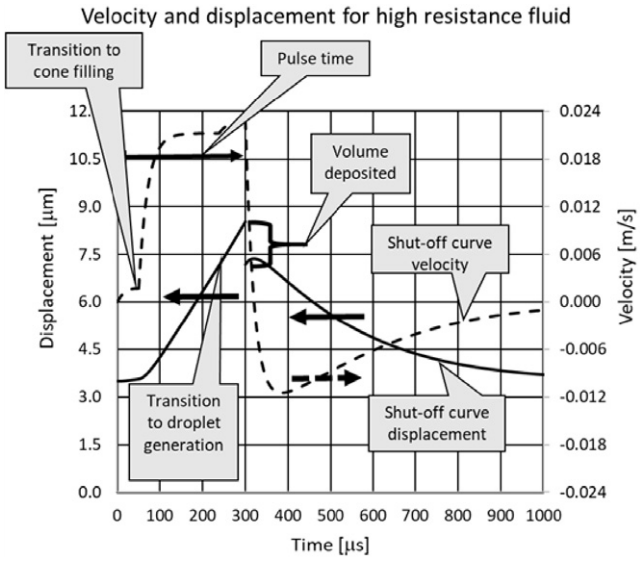

Figure 16. Results of calculations with a high resistance fluid $\mathbb{R}_{cap} = 7.07 \times 10^{10}$ Ω. Pulse length $t_{pulse} = 300$ µs. Jetting starts at $t = 239$ µs. The volume jetted equals 27 pL. During jetting the voltage drop in the nozzle is 324 V, still smaller than the applied voltage of 2800 V.

control appears to be a valuable and effective method to dispose small quantities of fluid out of a large nozzle. For our experiments, we used an electrically insulating glass capillary. In such a set-up, the electrical current has to flow through the liquid. Conduction in a liquid is governed by moving ions. Applying an electrical field in the fluid let the ions move. Moving ions generate drag. This is not the case in a system with a metal nozzle with a very low electrical resistance.

In order to describe the details of the process, understanding the effects of electrokinetic forcing is important. This force is generated by the ion current through the capillary between the tip of the electrode and the meniscus. During start-up, the current comes from loading the capacitors. This causes a "kick-start" of the fluid in the capillary. During the "kick-start," the dome-shaped equilibrium meniscus flips into a pseudo-Taylor cone. This is a cone with a larger aperture than the Taylor cone. During subsequent filling of the meniscus, the time rate of change in capacitance is not important. In between the kick-start and the start of the jetting only the static head, consisting of the hydrostatic pressure, the capillary pressure high up in the capillary and gauge pressure, and viscous drag must be taken into account in the equation of motion. Following G.I. Taylor jetting starts at the moment the cone shaped meniscus has reached the Taylor cone dimensions. A small jet starts issuing from the tip of the Taylor cone. This jet quickly decomposes into a stream of small droplets by the Rayleigh–Plateau–Weber instability. The velocity of the jet leaving the cone is a constant only depending on the viscosity, surface tension and the fraction of surface charge transported along with the jet. The current linked to the stream of charged droplets again loads the fluid inside the capillary through the electrokinetic effect and supports pumping the fluid through the capillary. Upon switching off the pulse, the electrokinetic force stops the fluid motion as it was an "emergency stop" and the fluid column slowly returns to static equilibrium. This allows driving on-demand electrohydrodynamic jetting up to say 1 kHz. Any frequency up to 1 kHz is allowed, making the process usable for printing patterns on a moving substrate.

The concept needed to understand why a meniscus can carry such a high voltage as reported about in this article is the Taylor cone. This concept can be also used for cones, called pseudo-Taylor cones, slightly different from the Taylor cone. This assumption makes it possible to calculate the capacitance during the filling of the meniscus and to calculate the "kick-start" effect.

The ion mobility is an important parameter. Choosing the right value of the ion mobility k is critical. Our hypothesis is that ions are generated at the tip of the electrode by electrolysis of water in the mixture with ethylene glycol. It is about hydrogen and hydroxyl ions. The value of k is inversely proportional to the viscosity. The data listed, for instance in Physical Chemistry handbook by Atkins [39] (Table 21.6 on page 1019), are valid for ions in water. The viscosity of the liquid used in this article equals 7.2 mPas. Moreover, the electrokinetic force is a body force, its effect on the fluid flow depends on the shape of the channel between the tip of the electrode and the nozzle front. For the calculations $k_{eff} = 1,28 \times 10^{-5}$ [m^2/(Vs)] has been entered. Using this value gives good agreement with experiments and this choice makes sense compared to the values in water for the mobility of hydrogen and hydroxyl ions.

On-demand electrohydrodynamic jetting is an extremely well-controllable process depending on the precise adjustment of the pulse, namely the pulse height and time. The slew rate of the power amplifier determines the "kick-off start" and "emergency stop" effects. It takes a while for the meniscus to adapt its shape prior to droplet formation. During the last part of the pulse, the velocity goes to a constant value; the displacement, however, increases indefinitely with time in a run-away manner. Importantly, the volume jetted can be controlled by the fluid height in the capillary and the pulse length.

This study describes the principle of on-demand electrohydrodynamic jetting with importance in applications beyond the fluid deposition in biosensor technologies.

6. APPENDICES

6.1 *Capacitance of Taylor Cone and Flat Plate*

In order to calculate the capacitance of a conducting cone kept at potential V_0 and a grounded conducting flat plate mounted at right angles with respect to the axis of the cone, we have adapted the theory developed by Taylor in his article on the "Disintegration of water droplets in an electrical field" [40]. The height of the cone measures h, its half the apex angle α. The distance between the tip of the cone and the plate is given by d. For the analysis a spherical co-ordinate system is defined. The origin is at the tip of the cone. See Figure 17.

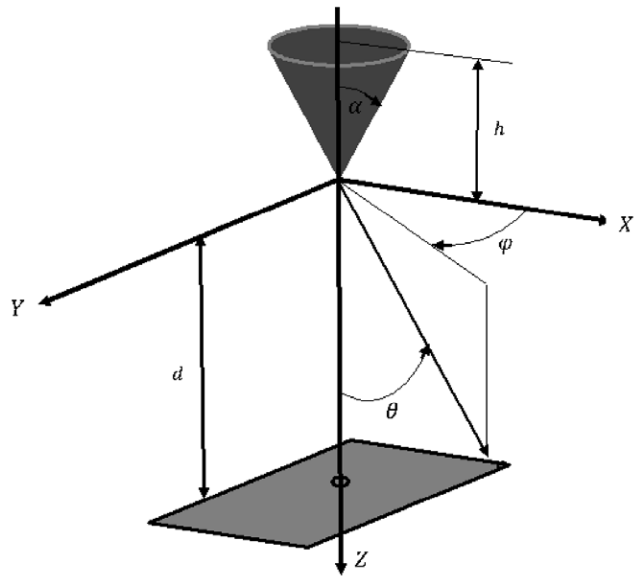

Figure 17. Cone defined with respect to spherical co-ordinate system $Or\theta\varphi$. The tip of the cone coincides with the origin of the co-ordinate system. The semi apex angle is denoted by α, the height by h. The distance of the apex of the cone to the plane is given by d.

G.I. Taylor's analysis starts with the observation that the tension due to an electrical field must balance the surface tension pressure on the surface of the fluid cone. The tension is given by ($\epsilon = \epsilon_r \epsilon_0$ and σ the charge density):

$$F = \frac{\sigma^2}{2\epsilon}.$$

This tension (unit pressure) counterbalances the surface tension pressure on the conical surface given by:

$$p_{\text{surface tension}} = \frac{\gamma}{r \tan\alpha}.$$

As σ is proportional to the derivative of the potential V, the potential along the surface of the cone should depend on $r^{1/2}$. The potential is the solution of a bipotential equation $\nabla.\nabla V = 0$, of which the solution can be expressed as:

$$U = U_0 + A r^{\frac{1}{2}} P_{\frac{1}{2}}(\cos\theta).$$

Here $P_{\frac{1}{2}}(\cos\theta)$ is the Legendre function of fractional order $1/2$. The cone consists of a conducting material, consequently the potential along the surface must be constant. This can only be reached for the angle θ_0 for which it holds:

$$P_{\frac{1}{2}}(\cos\theta_0) = 0.$$

From the "Handbook of Mathematical Functions" (8.13.11) [49], and from M.C. Gray's "Legendre Functions of Fractional order" ([50], formula 7) an expression is found that enables the evaluation of this function:

$$P_{\frac{1}{2}}(\cos\theta) = \frac{2}{\pi}\left[2E\left(\sin\frac{\theta}{2}\right) - K\left(\sin\frac{\theta}{2}\right)\right],$$

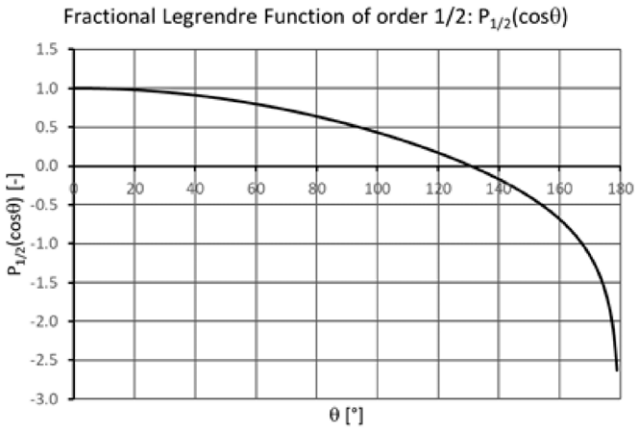

Figure 18. Fractional Legendre function $P_{\frac{1}{2}}(\cos\theta)$ as function of θ.

where E and K are the complete elliptic integrals of the first and second type, respectively. Using the approximate polynomial solutions given in "Handbook of Mathematical Functions" (17.3.34 and 17.3.36), the result is shown in Figure 18. For the sake of completeness the elliptic integrals are given here:

$$K(k) = \int_0^{\frac{\pi}{2}} \frac{d\vartheta}{\sqrt{1-k^2\sin^2\vartheta}}, \; E(k) = \int_0^{\frac{\pi}{2}} \sqrt{1-k^2\sin^2\vartheta}\, d\vartheta.$$

For the calculation of the charge density, the derivatives of the E and K functions with respect to θ are needed (see Byrd and Friedman, 710.00 and 710.02 [51]):

$$\frac{dK(x)}{dx} = \frac{E(x) - \left(1-x^2\right)K(x)}{x\left(1-x^2\right)}$$
$$\frac{dE(x)}{dx} = \frac{E(x) - K(x)}{2x}.$$

The derivative of the Legendre function reads:

$$\frac{\partial P_{\frac{1}{2}}(\cos\theta)}{\partial\theta} = \frac{1}{2\pi}\frac{1}{\tan\frac{\theta}{2}}\left[\frac{1-2\sin^2\frac{\theta}{2}}{1-\sin^2\frac{\theta}{2}}E\left(\sin\frac{\theta}{2}\right) - K\left(\sin\frac{\theta}{2}\right)\right].$$

The charge density on the cone $\theta = \theta_0$ follows from:

$$\sigma = \epsilon\frac{1}{r}\frac{\partial U}{\partial\theta} = \epsilon A r^{-\frac{1}{2}}\frac{\partial P_{\frac{1}{2}}(\cos\theta)}{\partial\theta}|_{\theta=\theta_0}.$$

With definition of tension and the formula for the surface tension, the equilibrium condition at the cone surface enables the calculation of A ($\alpha = \pi - \theta$):

$$\frac{\gamma}{r\tan\alpha} = \frac{1}{2}\frac{1}{\epsilon}\left[\epsilon A r^{-\frac{1}{2}}\frac{\partial P_{\frac{1}{2}}(\cos\theta)}{\partial\theta}|_{\theta=\theta_0}\right]^2$$
$$\frac{\gamma}{\tan\alpha} = \frac{1}{2}\epsilon\left[A\frac{\partial P_{\frac{1}{2}}(\cos\theta)}{\partial\theta}|_{\theta=\theta_0}\right]^2.$$

For free space from this equation A can be determined (Taylor result $\theta_0 = 130.71° = 2.281$ rad,):

$$\frac{\partial P_{\frac{1}{2}}(\cos\theta)}{\partial\theta}|_{\theta=\theta_0} = -0.9747,$$
$$\tan\alpha_0 = \tan(\pi - \theta_0) = \tan 49.29° = 1.1622$$
$$\epsilon = \epsilon_r\epsilon_0 = 8.85\times10^{-12}\left[\frac{F}{m}\right],$$
$$A = \pm 4.523\times10^5\sqrt{\gamma}\left[\frac{V}{\sqrt{m}}\right].$$

With the charge distribution now known, the total charge on the cone can be calculated:

$$Q = \int_0^{\frac{h}{\cos\alpha}} \sigma 2\pi r\sin\alpha dr = \epsilon 2\pi A\sin\alpha\frac{\partial P_{\frac{1}{2}}(\cos\theta)}{\partial\theta}|_{\theta=\theta_0}$$
$$\int_0^{\frac{R_{\text{nozzle}}}{\sin\alpha}} r^{\frac{1}{2}}drQ = 1.878\times10^{-5}R_{\text{nozzle}}\sqrt{\gamma R_{\text{nozzle}}}\,[C].$$

The total charge on the Taylor cone does not depend on the applied voltage and does not depend on the gap height D_g. It follows solely from the equilibrium between the surface tension and the electrostatic tension. Inside the cone the pressure equals zero. The capacitance of the fluid cone in equilibrium with the applied field is given by (free space):

$$C_{\text{cone}} = \frac{Q}{U} = \frac{1.878\times10^{-5}R_{\text{nozzle}}\sqrt{\gamma R_{\text{nozzle}}}}{U}\,[F].$$

As the capacitance of the cone does not depend on D_g, the capacitance force follows from:

$$F_{\text{cap,cone}} = \frac{1}{2}\frac{\partial C_{\text{cone}}}{\partial D_g}U^2 = 0.$$

The integral of electrostatic tension over the surface area of the cone is in equilibrium with the surface tension force acting along the rim of the cone attached to the rim of the nozzle and does not contribute to the capacitance force. This statement can be proved as follows. The electrostatic tension force is given by:

$$F_{\text{tension}} =$$
$$\int_0^{R_{\text{nozzle}}/\sin\alpha_0}\frac{1}{2}\epsilon\left(A\frac{\partial P_{\frac{1}{2}}(\cos\theta)}{\partial\theta}|_{\theta=\theta_0}\right)^2\frac{1}{r}2\pi r\sin^2\alpha_0 dr =$$
$$\pi\epsilon\left(A\frac{\partial P_{\frac{1}{2}}(\cos\theta)}{\partial\theta}|_{\theta=\theta_0}\right)^2 R_{\text{nozzle}}\sin\alpha_0 =$$
$$\pi\frac{2\gamma}{\tan\alpha_0}R_{\text{nozzle}}\sin\alpha_0 = 2\pi\gamma R_{\text{nozzle}}\cos\alpha_0.$$

The expression after the last equal sign is equal to the surface tension force acting upward along the rim to support the cone. As the generatrix of the cone is a straight line, charge does not influence the surface tension. This also means that the pressure inside the cone equals zero.

6.2 *Capacitance Pseudo-Taylor Cone*

The calculations so far are valid for the Taylor cone with $\theta_0 = 130.71° = 2.281$ rad, $\alpha_0 = 49.29°$. During charging, the cone starts at angles $\theta < \theta_0$, or $\alpha > \alpha_0$. Such a cone is referred to as a pseudo-Taylor cone. The potential is given by (A is a constant):

$$U = U_0 + Ar^\nu P_\nu(\cos\theta),$$

where $P_\nu(\cos\theta)$ a Legendre function of fractional order ν. For a Taylor cone $\nu = 1/2$. For a pseudo-Taylor cone with a larger half apex angle $\alpha > \alpha_0$: $\nu > 1/2$.
On the surface of the cone the potential is constant. This can only be true as long as:

$$P_\nu(\cos\theta) = 0.$$

Gray has given an approximate expression for $P_\nu(\cos\theta)$ using the recurrence formula [formula 1, $\nu = 1+\delta$]:

$$P_\nu(\cos\theta) =$$
$$\frac{(1+2\delta)\cos\theta - \delta}{1+\delta} + 2\delta\frac{(1+2\delta)\cos\theta+\delta}{1+\delta}\ln\cos\frac{1}{2}\theta.$$

From this expression the zero of $P_\nu(\cos\theta)$ can be derived ([50], formula 20):

$$\ln\left(\cos\frac{\theta}{2}\right) = -\frac{1}{2\delta}\frac{(1+2\delta)\cos\theta-\delta}{[(1+2\delta)\cos\theta+\delta]},\ \nu = 1+\delta.$$

For given α δ follows from a quadratic equation in δ. The root with the minus sign for the square root term makes sense.
The charge density on the cone surface follows from (see Gray [50], formula 26):

$$\frac{\partial P_\nu(\cos\theta)}{\partial\theta}|_{\theta=\pi-\alpha} = -\frac{2\delta(1+\delta)}{\sin\theta[(1+2\delta)\cos\theta+\delta]}$$
$$\sigma = \epsilon\frac{1}{r}\frac{\partial U}{\partial\theta} = \epsilon Ar^{\nu-1}\frac{\partial P_\nu(\cos\theta)}{\partial\theta}|_{\theta=\pi-\alpha}.$$

At the surface of the pseudo-Taylor cone, the electrostatic tension must be in equilibrium with the surface tension pressure and the internal pressure $p(r)$ in the cone (for the Taylor cone the internal pressure is zero):

$$\frac{\gamma}{r\tan\alpha} = p(r) + \frac{1}{2}\frac{\sigma^2}{\epsilon} =$$
$$p(r) + \frac{1}{2}\epsilon A^2r^{2(\nu-1)}\left[\frac{\partial P_\nu(\cos\theta)}{\partial\theta}|_{\theta=\pi-\alpha}\right]^2$$
$$p(r) = \frac{\gamma}{r\tan\alpha} - \frac{1}{2}\epsilon A^2r^{2(\nu-1)}\left[\frac{\partial P_\nu(\cos\theta)}{\partial\theta}|_{\theta=\pi-\alpha}\right]^2.$$

The constant A can be found by putting a condition on the pressure $p(r)$. Here it is assumed that the pressure generated by electrostatic forces at the entrance is zero $p(R_{\text{nozzle}}/\sin\alpha) = 0$. This leads to an expression for A:

$$A = \pm\frac{1}{\left(\frac{R_{\text{nozzle}}}{\sin\alpha}\right)^\nu\left[\frac{\partial P_\nu(\cos\theta)}{\partial\theta}|_{\theta=\pi-\alpha}\right]}\sqrt{2\frac{\gamma}{\epsilon}\frac{\cos\alpha}{R_{\text{nozzle}}}}.$$

With the constant A determined, the total charge on the pseudo-Taylor cone and its capacity can be found by evaluation of:

$$Q = \int_0^{\frac{R_{\text{nozzle}}}{\sin\alpha}} \sigma 2\pi r \sin\alpha dr = 2\pi\epsilon A \sin\alpha \int_0^{\frac{R_{\text{nozzle}}}{\sin\alpha}} r^{\nu} dr$$
$$= 2\pi\epsilon A R_{\text{nozzle}} \left[\frac{\partial P_{\nu}(\cos\theta)}{\partial\theta}|_{\theta=\pi-\alpha}\right] \frac{1}{\nu+1} \left(\frac{R_{\text{nozzle}}}{\sin\alpha}\right)^{\nu}$$
$$C_{\text{pseudo cone}} = \frac{Q}{U}.$$

Again, the total charge does not depend on the applied potential.

6.3 *Surface Tension Driven Meniscus Oscillations*

We will discuss two surface tension driven modes in the capillary: the slosh mode and the first higher-order mode.

Slosh-mode Frequency of a Wave Guide Type Print Head

The slosh-mode kinematics is characterized by the fact that the fluid column in the capillary (total length L) and nozzle (radius R_{nozzle}, cross-section $A_{\text{nozzle}} = \pi R_{\text{nozzle}}^2$ and length L_{nozzle}) moves against the spring action of the surface tension acting on the meniscus [43].

The capillary pressure is given by the Young–Laplace equation (with $a = R_1/\sin\theta_0$):

$$p_{\text{cap}} = \frac{2\gamma}{a} = 2\gamma \frac{\sin\theta_0}{R_{\text{nozzle}}}.$$

The force associated with the capillary pressure follows from:

$$F_{\text{cap}} = p_{\text{cap}} A_{\text{nozzle}} = 2\pi\gamma R_{\text{nozzle}} \sin\theta_0.$$

As all other force contributions are constant, the stiffness of the surface tension spring follows from:

$$C = \frac{\partial F_{\text{cap}}}{\partial x} = \frac{\partial F_{\text{cap}}}{\partial\theta_0}\frac{\partial\theta_0}{\partial x}.$$

The relation between the volume displacement x and θ_0 reads:

$$x = \frac{\text{Volume dome}}{\pi R_{\text{nozzle}}^2} = \frac{1}{3} R_{\text{nozzle}} \frac{2-\cos\theta_0-\cos^2\theta_0}{\sin\theta_0(1+\cos\theta_0)}.$$

From:

$$\frac{dx}{dx} = 1 = \frac{1}{3} R_{\text{nozzle}} \frac{d}{d\theta_0}\left[\frac{2-\cos\theta_0-\cos^2\theta_0}{\sin\theta_0(1+\cos\theta_0)}\right]\frac{d\theta_0}{dx}$$
$$= R_{\text{nozzle}} \frac{1}{(1+\cos\theta_0)^2}\frac{d\theta_0}{dx}.$$

We derive:

$$\frac{d\theta_0}{dx} = \frac{1}{R_{\text{nozzle}}}(1+\cos\theta_0)^2.$$

And the stiffness becomes:

$$C = \frac{\partial F_{\text{cap}}}{\partial x} = \frac{\partial F_{\text{cap}}}{\partial\theta_0}\frac{\partial\theta_0}{\partial x} = 2\pi\gamma\cos\theta_0(1+\cos\theta_0)^2.$$

The stiffness depends on θ_0. At a certain fixed position x_0 and small deviations $|\Delta x| \ll x_0$ C can be considered a constant and the equation of motion for small deviations from the fixed position can be derived and is given by (all motions scaled with respect to the surface area of the nozzle and viscous drag only present in the nozzle):

$$M = \rho\pi\left[R_{\text{cap}}^2(L-L_{\text{nozzle}})\frac{A_{\text{nozzle}}^2}{A_{\text{cap}}^2} + R_{\text{nozzle}}^2 L_{\text{nozzle}}\right],$$
$$K = 8\pi\mu L_{\text{nozzle}})$$
$$M\ddot{\Delta x} = -K\dot{\Delta x} - C\Delta x.$$

Although M and$K$ are constants, the stiffness C depends on x and therefore the equation of motion is non-linear. Only when the deviations from equilibrium are small C can be considered a constant, although depending on the value of x (and θ_0) and thus on the shape of the meniscus. This equation defines the undamped natural resonance frequency and damping factor:

$$f_{\text{slosh}} = \frac{1}{2\pi}\omega_0 = \frac{1}{2\pi}\sqrt{\frac{C}{M}} =$$
$$\frac{1}{2\pi}\sqrt{\frac{2\gamma\cos\theta_0(1+\cos\theta_0)^2}{\rho\left[R_{\text{cap}}^2(L-L_{\text{nozzle}})\frac{A_{\text{nozzle}}^2}{A_{\text{cap}}^2} + R_{\text{nozzle}}^2 L_{\text{nozzle}}\right]}}$$
$$\zeta = \frac{K}{2\sqrt{MC}}.$$

There is a direct relation between the viscous time constant τ_{viscous} and ζ:

$$\tau_{\text{viscous}} = \frac{M}{K} = \frac{1}{2\zeta\omega_0}.$$

Higher-order Symmetric Meniscus Oscillations

For higher-order meniscus resonance, we consider only fluid motions close to the meniscus; this is in contrast to the slosh mode for which all fluid in the system must be taken into account [52, 53]. The analysis will hold true for a frictionless fluid (dynamic viscosity $\mu = 0$). To describe the flow, a spherical co-ordinate system will be used with r, the co-ordinate measuring the distance from the meniscus away from the nozzle and θ, the angle measuring the distance from the center line of the nozzle. See Figure 19.

For the fundamental meniscus mode we pose the following ansatz:

$$w(r,t) = B[1+\lambda J_0(ka\theta)]\sin\omega t,\ w \ll R_{\text{nozzle}}.$$

The supposed small amplitude of the harmonic motion with radian frequency ω is given by $B[1+\lambda J_0(ka\theta)]$. $J_0(k\theta a)$ is a zeroth-order Bessel function of the first kind [54, 55]. The constant λ follows from the argument that at the rim of the nozzle wall the displacement of the meniscus equals zero:

$$\lambda = -\frac{1}{J_0(ka\theta_0)}.$$

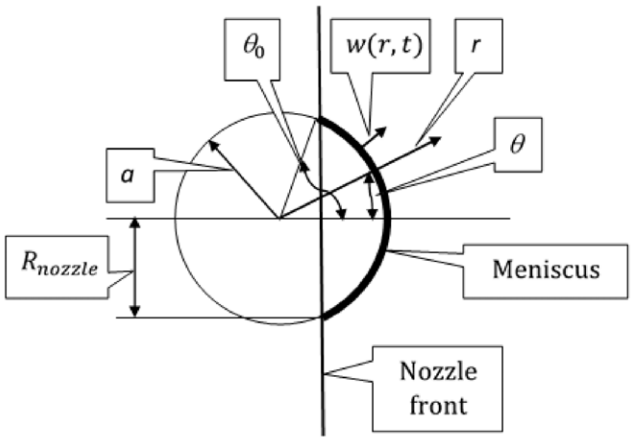

Figure 19. Definition of a spherical co-ordinate system attached to nozzle and meniscus.

The constant k is given by the fact that the fluid motion is local and that there is no net volume displacement (V volume, $a = R_{\text{nozzle}}/\sin\theta_0$):

$$V = 2\pi Ba^2 \int_0^{\theta_0} [1 + \lambda J_0(ka\theta)] \sin\theta \, d\theta =$$
$$2\pi Ba^2 \left[(1 - \cos\theta_0) + \lambda \int_0^{\theta_0} J_0(ka\theta) \sin\theta \, d\theta \right].$$

The integral cannot be solved in closed form, so we have to expand $\sin\theta$ into a Taylor series:

$$V \approx 2\pi Ba^2 \left[(1 - \cos\theta_0) + \lambda \int_0^{\theta_0} J_0(ka\theta) \left(\theta - \frac{1}{6}\theta^3 \right) d\theta \right].$$

The integral can now be found:

$$I = \int_0^{\theta_0} J_0(ka\theta) \left(\theta - \frac{1}{6}\theta^3 \right) d\theta$$
$$= \theta_0^2 \left\{ \begin{array}{c} \dfrac{J_1(ka\theta_0)}{ka\theta_0} - \\ \dfrac{\theta_0^2}{6} \dfrac{\left[2ka\theta_0 J_0(ka\theta_0) + \left((ka\theta_0)^2 - 4 \right) J_1(ka\theta_0) \right]}{(ka\theta_0)^3} \end{array} \right\}.$$

Substitution of the expression λ delivers the condition for which the volume V becomes zero:

$$\frac{\theta_0^2}{J_0(ka\theta_0)} \left\{ \begin{array}{c} (1 - \cos\theta_0) - \\ \dfrac{J_1(ka\theta_0)}{ka\theta_0} \\ - \dfrac{\theta_0^2}{6} \dfrac{\left[2ka\theta_0 J_0(ka\theta_0) + \left((ka\theta_0)^2 - 4 \right) J_1(ka\theta_0) \right]}{(ka\theta_0)^3} \end{array} \right\} = 0$$
$$\theta_0 < 1 : \theta_0^2 \left[\frac{1}{2} - \frac{J_1(ka\theta_0)}{ka\theta_0 J_0(ka\theta_0)} \right] = 0.$$

From these equations the value of $ka\theta_0 = k_1 a\theta_0$ can be found for which the net volume displacement equals zero. Also, the value of λ_1 is now known. The values for $ka\theta_0$ and λ_1 are listed in Table III for different values of θ_0.

Table III. The calculated values of $ka\theta_0$ and λ_1 for different values of θ_0. First approximation refers to result using the first term of the series expansion of $\sin\theta$, the second approximation to the inclusion of the third power of θ.

θ_0	$k_1 a\theta_0$ first approximation	$k_1 a\theta_0$ second approximation	λ_1 first approximation	λ_1 second approximation
0.01	5.1356	5.1356	7.56	7.56
0.1	"	5.1360	"	7.567
0.3	"	5.1386	"	7.618
0.6	"	5.1477	"	7.802
1	"	5.1712	"	8.323

Below $\theta_0 = 0.1$ there is hardly any difference between the first and second approximation.

The displacement and velocity distributions at the meniscus surface are given by:

$$w(\theta) = B[1 + \lambda_1 J_0(k_1 a\theta)] \sin\omega t$$
$$\frac{\partial w(\theta)}{\partial t} = \omega B[1 + \lambda_1 J_0(k_1 a\theta)] \cos\omega t$$

Suppose the component of the velocity vector in the fluid in radial r direction away from the meniscus is (separation of variables):

$$v_r(r, \theta, t) = \omega B F(r)[1 + \lambda_1 J_0(k_1 a\theta)] \cos\omega t, F(a) = 1.$$

Using the equation of continuity, the component of the velocity vector in θ-direction can be determined:

$$\frac{1}{r^2}\frac{\partial}{\partial r}\left(r^2 v_r\right) + \frac{1}{r\sin\theta}\frac{\partial}{\partial\theta}(v_\theta \sin\theta) = 0$$
$$v_\theta(r, \theta, t) = -\omega B \left[2rF(r) + r\frac{dF(r)}{dr} \right]$$
$$\frac{\theta^2}{\sin\theta} \left[\frac{1}{2} + \frac{\lambda_1}{k_1 a\theta} J_1(k_1 a\theta) \right] \cos\omega t$$
$$\theta_0 < 1 : v_\theta(r, \theta, t) = -\omega B \left[2rF(r) + r\frac{dF(r)}{dr} \right]$$
$$\theta \left[\frac{1}{2} + \frac{\lambda_1}{k_1 a\theta} J_1(k_1 a\theta) \right] \cos\omega t.$$

Substitution of the expressions for the components of the velocity vector into the components of the equation of motion yields (neglecting viscosity and skipping the convective terms, this last action can be justified by the fact that only small deviations from the equilibrium meniscus position are considered, so B small):

$$-\rho\omega^2 BF(r)[1 + \lambda_1 J_0(k_1 a\theta)] \sin\omega t = -\frac{\partial p}{\partial r}$$
$$\rho\omega^2 B \left[2rF(r) + r\frac{dF(r)}{dr} \right] \theta \left[\frac{1}{2} + \frac{\lambda_1}{k_1 a\theta} J_1(k_1 a\theta) \right]$$
$$\sin\omega t = -\frac{1}{r}\frac{\partial p}{\partial\theta}.$$

Differentiation of the r-component of the equation of motion with respect to θ and differentiation of the

θ-component of the equation of motion with respect to r yields:

$$\rho\omega^2 BF\,(r)\,[\lambda_1 k_1 \mathrm{a} J_1\,(k_1 a\theta)]\sin\omega t = -\frac{\partial^2 p}{\partial r\partial\theta}$$
$$\rho\omega^2 B\left[2F\,(r) + 4r\frac{dF\,(r)}{dr} + r^2\frac{d^2F\,(r)}{dr^2}\right]\theta$$
$$\left[\frac{1}{2} + \frac{\lambda_1}{k_1 a\theta}J_1\,(k_1 a\theta)\right]\sin\omega t = -\frac{\partial^2 p}{\partial\theta\partial r}.$$

We remove the dependence on r in both equations by averaging over θ from $\theta = 0$ to $\theta = \theta_0$ (by definition $\lambda_1 J_0\,(k_1 a\theta_0) = -1$, for the first order approximation $k_1 a\theta_0 = 5.1356$) and the function F must obey:

$$\left[2 - \frac{(k_1 a)^2}{1 + \frac{1}{4}\,(k_1 a\theta_0)^2}\right]F\,(r) +$$
$$4r\frac{dF\,(r)}{dr} + r^2\frac{d^2F\,(r)}{dr^2}0,\ F\,(a) = 1.$$

This differential equation can be solved by standard means:

$$F = \left(\frac{r}{a}\right)^{\nu},\ \nu = \frac{-3 + \sqrt{1 + 4\left[\frac{(k_1 a)^2}{1+\frac{1}{4}(k_1 a\theta_0)^2}\right]}}{2}$$
$$= \frac{-3 + \sqrt{1 + 0.52676\,(k_1 a)^2}}{2}.$$

The function F vanishes for $r \to 0$. Indeed, the fluid motion belonging to the first axisymmetric higher-order oscillatory mode has a limited reach. The components of the velocity vector are:

$$v_r\,(r,\theta,t) = \omega B\left(\frac{r}{a}\right)^{\nu}[1 + \lambda_1 J_0\,(k_1 a\theta)]\cos\omega t,$$
$$v_\theta\,(r,\theta,t) =$$
$$\omega B\,(2+\nu)\left(\frac{r}{a}\right)^{\nu}\theta\left[\frac{1}{2} + \frac{\lambda_1}{k_1 a\theta}J_1\,(k_1 a\theta)\right]\cos\omega t.$$

In order to calculate the resonance frequency, we make use of Rayleigh's principle [56]. This principle states that for a harmonically moving non-damped system (no viscous losses), the sum of the potential energy and the kinetic energy stays constant. The potential energy is the excess surface energy and will be calculated at maximum deformation of the meniscus using a kinematic plausible guess of the deformation of the meniscus. For the kinetic energy a dynamic plausible estimate of the inner deformation field of the fluid dome evaluated at maximum deformation rate (no deformation of meniscus) will be used.

The maximum potential energy equals the increase in surface energy at maximum displacement ($\omega t = \pi/2 + n\pi$, $n = 1, 2, \ldots$). With respect to the spherical co-ordinate system we have:

$$U_{max} = \gamma\,\Delta A_{max}$$
$$\Delta A_{max} = 2\pi\int_0^{\theta_0}(a+w)^2\sin\theta\sqrt{1 + \frac{1}{(a+w)^2}\left(\frac{dw}{d\theta}\right)^2}$$
$$d\theta - 2\pi a^2\int_0^{\theta_0}\sin\theta\,d\theta.$$

For $w \ll a$ and neglecting all small terms of higher order we arrive at:

$$= 2\pi\int_0^{\theta_0}\left(a^2 + 2aw\right)\sin\theta\left[1 + \frac{1}{2}\frac{1}{a^2}\left(\frac{dw}{d\theta}\right)^2\right]$$
$$d\theta - 2\pi a^2\int_0^{\theta_0}\sin\theta\,d\theta.$$

As the cross term aw equals zero by definition the final result reads:

$$\Delta A_{max} = \pi\int_0^{\theta_0}\left(\frac{dw\,(\theta)}{d\theta}\right)^2\sin\theta\,d\theta =$$
$$\pi B^2\lambda_1^2\,(k_1 a)^2\int_0^{\theta_0}J_1^2\,(k_1 a\theta)\sin\theta\,d\theta \approx$$
$$\pi B^2\lambda_1^2\,(k_1 a)^2\int_0^{\theta_0}J_1^2\,(k_1 a\theta)\,\theta\,d\theta =$$
$$\pi B^2\lambda_1^2\frac{k_1 a\theta_0}{2}\begin{bmatrix}k_1 a\theta_0 J_0^2(k_1 a\theta_0) + k_1 a\theta_0 J_1^2(k_1 a\theta_0) - \\ 2J_0\,(k_1 a\theta_0)\,J_1\,(k_1 a\theta_0)\end{bmatrix} = 273B^2.$$

The maximal kinetic energy calculated at $\omega t = 0 + n\pi$, $n = 1, 2, \ldots$ evaluated with respect to the cylindrical co-ordinate system is given by:

$$T_{max} = \frac{1}{2}\rho 2\pi\int_0^a\int_0^{\theta_0}\left(v_r^2 + v_\theta^2\right)r^2\sin\theta\,dr\,d\theta$$
$$\approx \frac{1}{2}\rho 2\pi\int_0^a\int_0^{\theta_0}\left(v_r^2 + v_\theta^2\right)r^2\theta\,dr\,d\theta.$$

Per velocity component the contributions to the kinetic energy are calculated:

$$T_{max,v_r} = \frac{\pi}{(3+2\nu)}\rho\omega^2 B^2 a^3\theta_0^2$$
$$\left\{\frac{1}{2} + \frac{2\lambda_1}{k_1 a\theta_0}J_1\,(k_1 a\theta_0) + \frac{\lambda_1^2}{2}\left[J_0^2\,(k_1 a\theta_0) + J_1^2\,(k_1 a\theta_0)\right]\right\}$$
$$T_{max,v_\theta} = \pi\frac{\left(4 + 4\nu + \nu^2\right)}{3+2\nu}\rho\omega^2 B^2 a^3\theta_0^4$$
$$\left\{\begin{array}{c}\frac{1}{16} + \frac{\lambda_1}{(k_1 a\theta_0)^3}\left[2J_1\,(k_1 a\theta_0) - k_1 a\theta_0 J_0\,(k_1 a\theta_0)\right] \\ +\frac{1}{2}\frac{\lambda_1^2}{(k_1 a\theta_0)^3}\begin{bmatrix}k_1 a\theta_0 J_0^2\,(k_1 a\theta_0) + k_1 a\theta_0 J_1^2\,(k_1 a\theta_0) \\ -2J_0\,(k_1 a\theta_0)\,J_1\,(k_1 a\theta_0)\end{bmatrix}\end{array}\right\}.$$

Substituting the equations for v_z and v_z after a lengthy calculation involving many manipulations with integrals involving Bessel functions and products of Bessel

functions [55], the maximum kinetic energy becomes:

$$T_{max} = f\ (\theta_0)\ \rho B^2 \omega^2 R^3_{\text{nozzle}}.$$

Applying Rayleigh's theorem we find for different angles:

$$\theta_0 = 1:\ U_{max} = T_{max} \rightarrow f_1 = 1.096\sqrt{\frac{\gamma}{\rho R^3_{\text{nozzle}}}}\,[\text{Hz}]$$

$$\theta_0 = 0.5:\ U_{max} = T_{max} \rightarrow f_1 = 1.334\sqrt{\frac{\gamma}{\rho R^3_{\text{nozzle}}}}\,[\text{Hz}]$$

$$\theta_0 \leq 0.1:\ U_{max} = T_{max} \rightarrow f_1 = 1.433\sqrt{\frac{\gamma}{\rho R^3_{\text{nozzle}}}}\,[\text{Hz}].$$

For a nozzle of 50 μm diameter and the test fluid used in this article ($\gamma = 0.0554$ N/m and $\rho = 1079$ kg/m^3), the resonance frequencies for the cases listed above are 63 kHz, 76.5 kHz and 82 kHz, respectively.

REFERENCES

[1] G. Joos, "Lehrbuch der Theoretischen Physik", Akademischer Verlagsgesellschaft Geest & Portig K.-G, Leipzig (1964), Viertes Buch, erstes Kapitel.

[2] A. J. Hijano, I. G. Loscertales, S. E. Ibáñez, and F. J. Higuera, "Periodic emission of droplets from an oscillating electrified meniscus of a low-viscosity, highly conductive liquid," A Phys. Rev. E **91**, 013011 (2015).

[3] J. Rosell-Llompart, J. Grifoll, and I. G. Loscertales, "Electrosprays in the cone-jet mode: From Taylor cone formation to spray development," J. Aerosol Sci. **125**, 2–31 (2018).

[4] C. U. Yurteri, R. P. A. Hartman, and J. C. M. Marijnissen, "Producing pharmaceutical particles via electrospraying with an emphasis on nano and nano structured particles - A review," Powder and Particle J. **28**, 91–115 (2010).

[5] U. Stachewicz, J. F. Dijksman, C. U. Yurteri, and J. C. M. Marijnissen, "Experiments on single event electrospraying," Appl. Phys. Lett. **91**, 254109 (2007).

[6] U. Stachewicz, "Single event AC-DC electrospraying," J. Phys. Conf. Ser. **142**, 012043 (2008).

[7] U. Stachewicz, J. F. Dijksman, D. Burdinski, C. U. Yurteri, and J. C. M. Marijnissen, "Relaxation times in single event electrospraying controlled by nozzle surface modification," Langmuir **25**, 2540–2549 (2009).

[8] U. Stachewicz, J. F. Dijksman, C. U. Yurteri, and J. C. M. Marijnissen, "Stability regime of pulse frequency for single event electrospraying," Appl. Phys. Lett. **95**, 224105 (2009).

[9] U. Stachewicz, J. F. Dijksman, C. U. Yurteri, and J. C. M. Marijnissen, "Volume of liquid deposited per single event electrospraying controlled by nozzle front surface modification," Microfluidics and Nanofluidics **9**, 635–644 (2010).

[10] U. Stachewicz, C. U. Yurteri, J. F. Dijksman, and J. C. M. Marijnissen, "Single event electrospraying of water," J. Aerosol Science **41**, 963–973 (2010).

[11] U. Stachewicz, "*Analysis of Electrospraying as an On-demand Deposition Method*," Thesis (Delft University of Technology, 2010) Chapter 5.

[12] D. Duft, T. Achtzehn, R. Mueller, and B. A. Huber, "Rayleigh jets from levitated microdroplets," Nature **421**, 128 (2003).

[13] R. T. Collins, K. Sambath, M. T. Harris, and O. A. Basaran, "Uniceesal scaling laws for the disintergration of electrifies drops," PNAS **110**, 4905–4910 (2013).

[14] J. W. S. Rayleigh, "On the instability of a cylinder of viscous liquid under capillary force," Philos. Mag. **34**, 145 (1892).

[15] C. Weber, "Zum zerfall eines Flüssigkeitsstrahles," Z. Angew. Math. Mech. **11**, 136–154 (1931).

[16] S. Middleman, *Modeling Axisymmetric Flows Dynamics of Films, Jets, and Drops* (Academic Press, New York, 1995), p. 165.

[17] J. M. Montanero and A. M. Cañán-Calva, "Dripping, jetting and tip-streaming," Reports on Progress in Phys. **83**, 097001 (2020).

[18] P. Atkins and J. de Paula, *Atkins Physical Chemistry* (Oxford University Press, New York, 2006), chapter 21.7.

[19] R. P. A. Hartman, D. J. Brunner, J. C. M. Marijnissen, and B. Scarlett, J. Aerosol. Sci. **29**, S977–S978 (1998).

[20] I. G. Loscertales, A. Barrero, M. Márquez, R. Spretz, R. Velarde-Ortiz, and G. Larsen, "Electrically forced coaxial nanojets for one-step hollow nanofiber design," J. Am. Chem. Soc. **126**, 5376–5377 (2004).

[21] K. Rahman, K. Ali, N. M. Muhammad, M-t Hyan, and K-h Choi, "Fine resolution drop-on-demand electrohydrodynamic patterning of conductive silver tracks on glass substrate," Appl. Phys. A **111**, 593–600 (2013).

[22] C.-H. Chen, G. Martin, and I. Hutchings, "Interaction of sequential pulsed electrohydrodynamic jets in drop-on-demand printing," *Proc. IS&T Printing for Fabrication 2016 (NIP32) 32nd Int'l. Conf. on Digital Printing Technologies* (IS&T, Springfield, VA, 2016), pp. 71–74.

[23] T.-H. Phung, "An elecrohydrodynamic (EHD) jet printing method for increasing print speed," *Proc. IS&T Printing for Fabrication 2017 (NIP33) 33nd Int'l. Conf. on Digital Printing Technologies* (IS&T, Springfield, VA, 2017), pp. 71–74.

[24] W. Liu, L. Zhu, C. Huang, and X. Jin, "Direct electrospinning of ultrafine fibers with interconnected macropores enabled by in situ mixing microfluidics," ACS Appl. Mater. & Interfaces **8**, 34870–34878 (2016).

[25] J. U. Park, M. Hardy, S. Kang, K. Barton, K. Adair, D. K. Mukhopadhyay, C. Y. Lee, M. S. Strano, A. G. Alleyne, J. G. Georiadis, P. M. Ferreira, and J. A. Rogers, "High-resolution electrohydrodynamic jet printing," Nature Mater **6**, 782–789 (2007).

[26] P. K. Szewczyk and U. Stachewicz, "The impact of relative humidity on electrospun polymer fibers: from structural changes to fiber morphology," Adv. Colloid and Interface Sci. **286**, 102315 (2020).

[27] D. P Ura, J. Rosell-Llompart, A. Zaszczyńska, G. Vasilyev, A. Gradys, P. K. Szewczyk, J. Knapczyk-Korczak, R. Avrahami, A. O. Šišková, A. Arinstein, P. Sajkiewicz, E. Zussman, and U. Stachewicz, "The role of electrical polarity in electrospinning and on the mechanical and structural properties of as-spun fibers," Materials **13**, 4169 (2020).

[28] J. Xue, T. Wu, Y. Dai, and Y. Xia, "Electrospinning and electrospun nanofibers: methods, materials, and applications," Chemical Reviews **119**, 5298–5415 (2019).

[29] S. Metwally, S. Ferraris, S. Spriano, Z. J. Krysiak, Ł. Kaniuk, M. M. Marzec, S. K. Kim, P. K. Szewczyk, A. Gruszczyński, M. Wytrwal-Sarna, J. E. Karbowniczek, A. Bernasik, S. Kar-Narayan, and U. Stachewicz, "Surface potential and roughness controlled cell adhesion and collagen formation in electrospun PCL fibers for bone regeneration," Mater. & Design **194**, 108915 (2020).

[30] Z. J. Krysiak, J. Knapczyk-Korczak, G. Maniak, and U. Stachewicz, "Moisturizing effect of skin patches with hydrophobic and hydrophilic electrospun fibers for atopic dermatitis," Colloids and Surfaces B: Biointerfaces **199**, 111554 (2021).

[31] A. Luraghi, F. Peri, and L. Moroni, "Electrospinning for drug delivery applications: A review," J. Controlled Release **334**, 463–484 (2021).

[32] T. Busolo, D. P. Ura, S. K. Kim, M. M. Marzec, A. Bernasik, U. Stachewicz, and S. Kar-Narayan, "Surface potential tailoring of PMMA fibers by electrospinning for enhanced triboelectric performance," Nano Energy **57**, 500–506 (2019).

[33] J. Knapczyk-Korczak, D. P. Ura, M. Gajek, M. M. Marzec, K. Berent, A. Bernasik, J. P. Chiverton, and U. Stachewicz, "Fiber-based composite meshes with controlled mechanical and wetting properties for water harvesting," ACS Appl. Mater. & Interfaces **12**, 1665–1676 (2019).

[34] A. Ivanoska-Dacikj and U. Stachewicz, "Smart textiles and wearable technologies–opportunities offered in the fight against pandemics in relation to current COVID-19 state," Rev. Advanced Mater. Sci. **59**, 487–505 (2020).

[35] R. P. A. Hartman, "*Electrodynamic atomization in the cone-jet mode. From physical modelling to powder production*". Thesis (University of Delft, 1998).

[36] MEGlobal Ethylene Glycol Product guide 2008.

[37] P. G. de Gennes, F. Brochart-Wyart, and D. Quéré, *Capillarity and Wetting Phenomena* (Springer, Berlin, 2002).
[38] W. R. Smythe, *Static and Dynamic Electricity*, 2nd ed. (MacGraw-Hill Book Company, 1950).
[39] P. Atkins and J. de Paula, *Atkins Physical Chemistry*, 8th ed. (Oxford University Press, New York, 2006), chapter 21.
[40] G. I. Taylor, "Disintegration of water drops in an electric field," Proc. R. Soc. London A **280**, 383–397 (1964).
[41] Hütte, Des Ingenieurs Taschenbuch, Theoretische Grundlagen, (Berlin 1955), p. 74.
[42] Hütte, Des Ingenieurs Taschenbuch, Theoretische Grundlagen, pp. 263–283.
[43] J. F. Dijksman, *Design of Piezo Inkjet Print Heads, from Acoustics to Applications* (Wiley VCH, New York, 2018), chapter 5.
[44] N. Fuchikami, S. Ishioka, and K. Kiyono, "Simulation of a dripping faucet," J. Phys. Soc. Japan **68**, 1185–1196 (1999) NL3501.
[45] T. Katsuyama and K. Nagata, "Behavior of the dripping faucet over a wide range of the flow rate," J. Phys. Soc. Japan **68**, 396–400 (1999).
[46] K. Kiyono and N. Fuchikami, "Dripping faucet dynamics by an improved mass-spring model," J. Phys. Soc. Japan **68**, 3259–3270 (1999).
[47] P. Martien, S. C. Pope, P. L. Scott, and R. S. Shaw, "The chaotic behavior of the leaky faucet," Phys. Lett. A **110**, 399–404 (1985).
[48] R. B. Bird, W. E. Stewart, and E. N. Lightfoot, *Transport Phenomena*, 2nd edn (John Wiley & Sons, New York, 2002), p. 848.
[49] M. Abramowitz and I. A. Stegun, *Handbook of Mathematical Functions* (Dover Publications, New York, 1970), Chapters 8 and 17.
[50] M. C. Gray, "Legendre functions of fractional order," Quart. App. Math. **11**, 311 (1953).
[51] P. F. Byrd and M. D. Friedman, *Handbook of Elliptic Integrals for Engineers and Scientists* (Springer-Verlag, Berlin, Heidelberg, New York, 1971).
[52] P. C. Duineveld and J. F. Dijksman, *Ultra Small Droplet Generation in Inkjet Printing by Higher Order Meniscus Oscillations, Proc. IS&T Printing for Fabrication 2018* (IS&T, Springfield, VA, 2018), pp. 147–150.
[53] J. Frits Dijksman and P. C. Duineveld, *Surface Tension Driven Meniscus Oscillations and the Effects on Droplet Formation, Proc. IS&T Printing for Fabrication 2019* (IS&T, Springfield, VA, 2019), pp. 83–88.
[54] M. Abramowitz and I. A. Stegun, *Handbook of Mathematical Functions* (Dover Publications, New York, 1970), Chapters 8 and 17, chapter 9.
[55] W. Rosenheinrich, "Tables of some indefinite integrals of bessel functions," Ernst Abbe Hochschule Jena University of Applied Sciences Germany 19.09.2015.
[56] J. W. Strutt and B. Rayleigh, *The Theory of Sound* (Dover Publications, New York, 1945), Vol. 1, pp. 109–110.